Radiosonde campaign in Paranal Observatory 2011: PWV measurement.

Omar Cuevas, Arlette Chacón & Michel Curé

AstroMeteorology group, Physics and Astronomy Department, Universidad de Valparaíso, Chile.

1 Introduction

The AstroMeteorology[1] group participated in a project conducted by ESO[2] in order to upgrade VISIR[3] instrumentation at the Paranal observatory. The main objective was the measurement of the Precipitable Water Vapor (PWV) by radiosonde launching from Paranal and comparing it with ground based instruments and numerical simulations.

In the 2009 the AstroMeteorology group participated in a similar measurement campaign at La Silla, Paranal and ALMA observatories in four campaigns. The principal objective of those campaign were to characterize the PWV in the astronomical sites of ESO in Chile, where we applied the WRF model to test the forecast of PWV and the standard meteorological variables.

For this campaign our AstroMeteorology group developed a meteorologic study with the data collected by radiosondes. The synoptic analysis reveled the importance of the knowledge of meteorological pattern in the zone and how the episodes of the "good and bad" PWV can be explained using traditional meteorology techniques. Also we numerically simulated the weather conditions during the campaign period using the WRF mesoscale meteorological model, compared the results from a synoptic point of view and evaluated it using statistical techniques with every radiosonde collected data.

The relevant results show the good performance of the WRF model to simulate and forecast the PWV episodes, at both the synoptic and local weather scales.

1.1 SOW

The AstroMeteorology group was invited by ESO to participate in the upgrade of the VISIR instrument in VLT Observatory. The SOW[4] document states that AstroMeteorology group is in charge of operations of the radiosonde campaign, of the delivery of the data and the atmospheric simulations with WRF model and of reposting the results. According to SOW document this report is a deliverable to ESO as part of the contract.

[1] *Avenida Gran Bretaña 1111, Valparaíso, Chile. Contact: omar.cuevas@uv.cl - michel.cure@uv.cl*
[2] European Southern Observatory
[3] http://www.eso.org/sci/facilities/paranal/instruments/visir/index.html
[4] VLT-SOW-ESO-14330-5504

2 Acronyms and Abbreviations

A	Anticyclonic
AP	Subtropical Anticyclonic Predominance
AW	Altiplanic Winter
B	cyclonic
BIAS	Error estimator
CL	Coastal Low
CORR	Statistical Correlation
F	Forecast
FNL	Final GFS Analysis
GFS	Global Forecast System
hPa	hectopascal
IR	Infrared satellite image
JS	Jet Stream
MYJ	Mellor-Yamada-Janjic
PBL	Planetary Boundary Layer
PWV	Precipitable Water Vapor
RMSE	Root Mean Square Error
u	component West-East of wind
UTC	Universal Time Coordinated
v	component North-South of wind
WRF	Weather Research and Forecasting model
YSU	Yensei-University

3 Radiosonde launching

The radiosonde campaign was successful in all the technical aspects; the logistic, materials, tools and helium worked perfectly. The communications with the aeronautic authority (Dirección de Aeronautica Civil) worked without problems. The launching zone was on the satellite communication antenna, located at 46 meters down of UT's telescopes.

Over 90% of the radiosonde launching schedule was launched on time. In just 2 cases, the launches were canceled by decisions from the campaign supervisor who estimated that the meteorological conditions could cause danger to the telescopes. Figure 1 shows the warning zone and the two cases aborted were affected by these, because the wind directions in the launching zone was from 225^{o} +- 25^{o}.

Finally, the schedule of the radiosondes launched successfully are presented in Table 1, where marked in red are the canceled cases.

Launch N^{o}	Date	Time (UTC)	Altitude Reached (m)	Distance Traveled (Km)	Last direction (^{o})
1	24-10-2011	00	23.240	101	95
2	25-10-2011	00	24.003	94	65
3	25-10-2011	12	26.543	103	61
4	26-10-2011	00	24.894	89,5	65
5	26-10-2011	12	21.237	92	68
6	27-10-2011	00	20.601	78,2	75
7	27-10-2011	12	27.180	78,5	80
8	28-10-2011	00	26.721	78,4	87
9	28-10-2011	12	25.612	55,2	101
10	29-10-2011	00	27.683	68,4	95
11	29-10-2011	12	27.605	68.2	90
12	30-10-2011	00	27.397	69,7	102
13	30-10-2011	12	26.777	76,2	99
14	31-10-2011	00	27.477	79,4	98
15	31-10-2011	12	26.603	96	93.6
16	01-11-2011	00	26.538	72,9	96
17	01-11-2011	12	25.880	89,1	92
18	02-11-2011	00	canceled	canceled	canceled
19	02-11-2011	12	25.446	70,3	80
20	03-11-2011	00	canceled	canceled	canceled
21	03-11-2011	12	24.407	65,8	81
22	04-11-2011	00	25.037	57	78
23	04-11-2011	12	25.901	48,8	69

Table 1: Radiosonde launching schedule. In red the canceled launchings by dangerous wind direction.

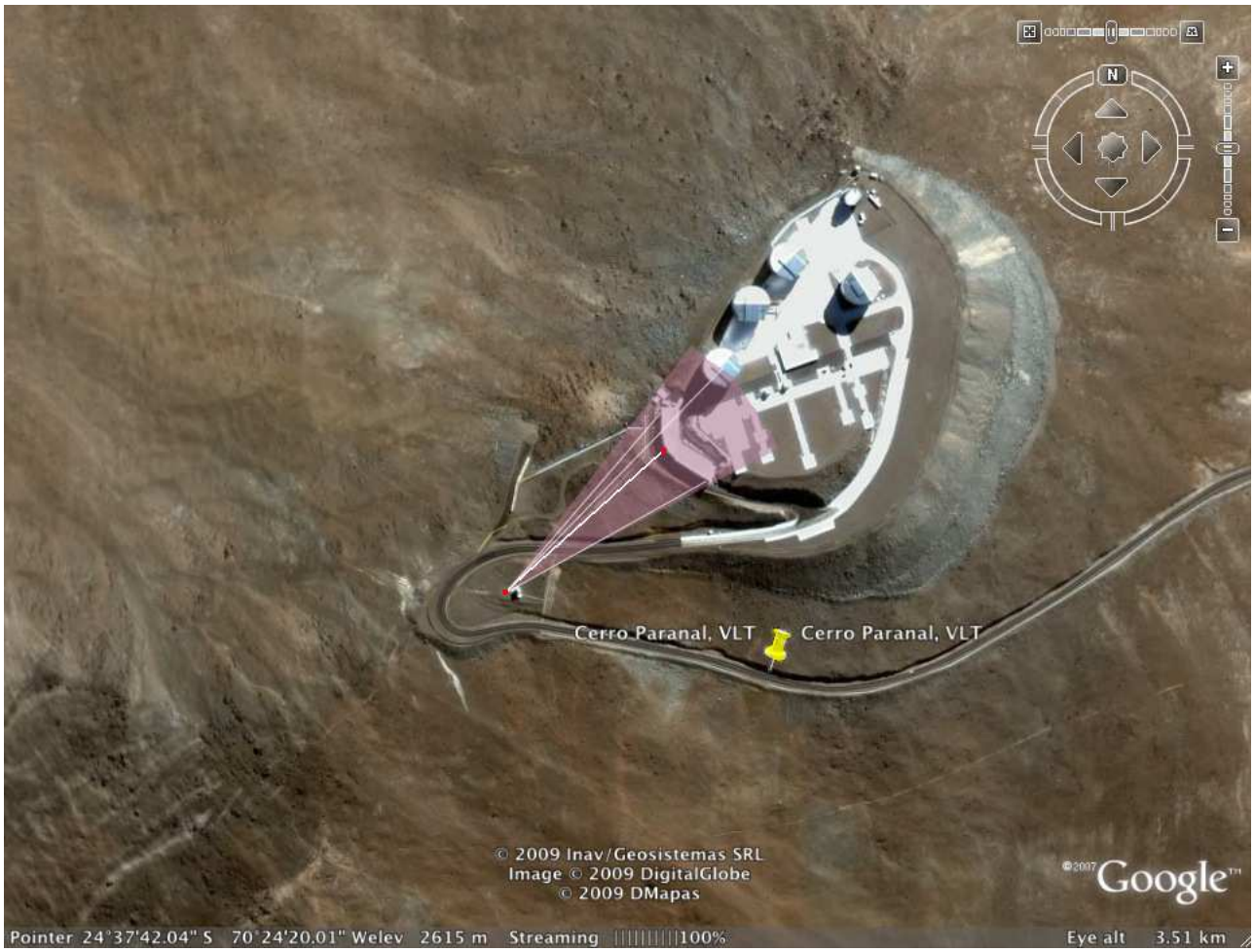

Figure 1: Warning zone for radiosonde launching. Location: -24 37' 45.3" South and -70 24' 23.5" West at 2584 m.a.s.l.

4 Meteorological pattern

4.1 Climatological description

The meteorological conditions in the north of Chile are very stable, where the desert conditions dominate the zone around Paranal with low humidity. The Subtropical Anticyclonic of the South Pacific rules has primary influence over this area, with clear sky most of the year. Between November and February (warm season), this condition changes when the Altiplanic Winter activity starts in the South Hemisphere (Figure 2). The Altiplanic Winter provokes atmospheric instability in the Cordillera de Los Andes, the principal storm activities are presented in the high hills of the East of Paranal.

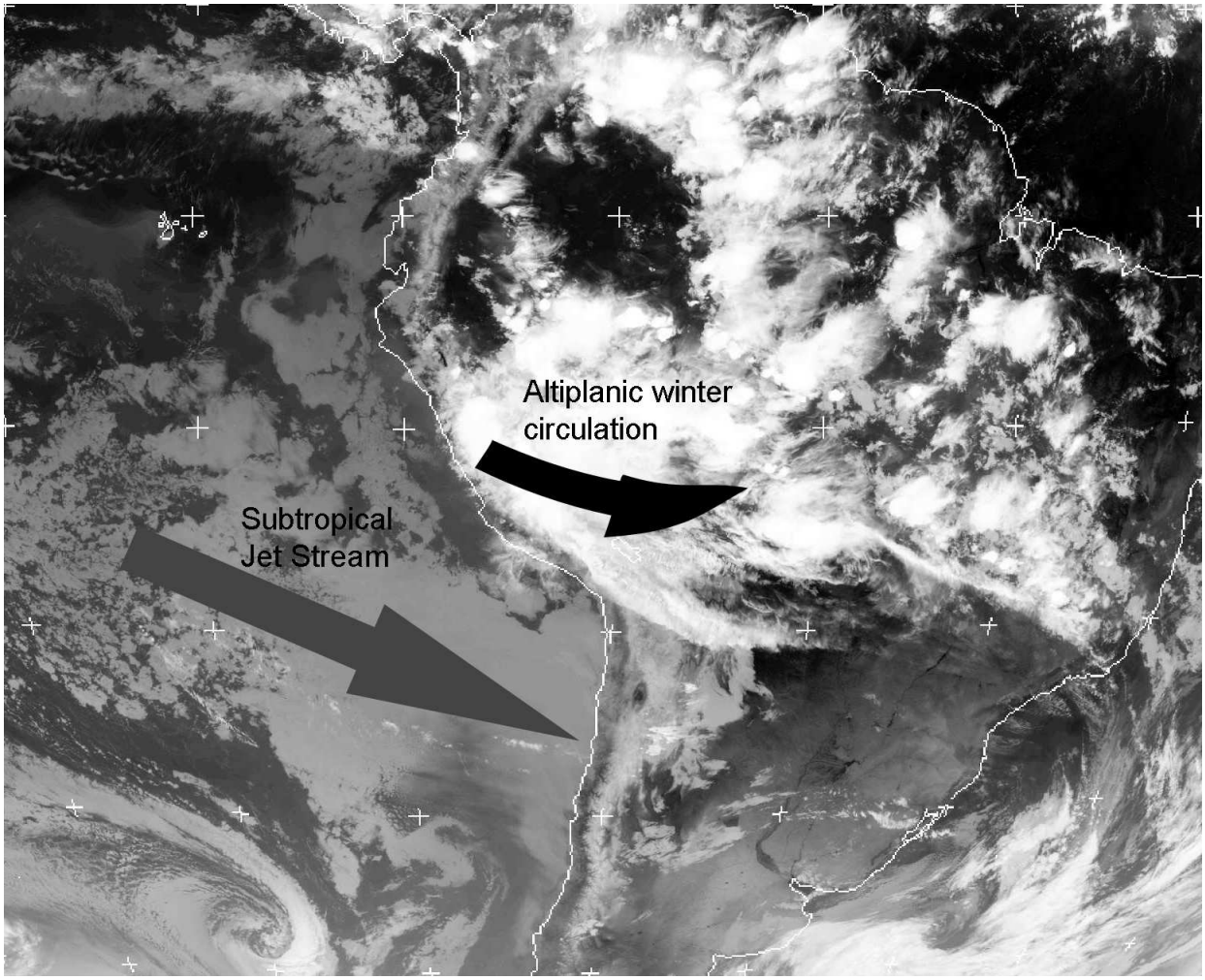

Figure 2: Altiplanic Winter case. IR satellite image at 00UTC-27/10/2011. *Source GOES-12.*

4.2 Synoptic patterns

During the radiosonde campaign developed in Paranal, the synoptic conditions were determined by the Altiplanic Winter, Jet Stream, Coastal Low and Subtropical Anticyclonic predominance.

In the 12 days of campaign, the PWV measured by the radiosonde show that the variation of its values were dominated by the weather conditions: lows values were influenced by Anticyclonic predominance, wind flow from the West and low local humidity. However, the high values of the PWV were influenced mainly from the Altiplanic Winter humidity advection by the Jet Stream.

The vertical distribution of PWV (Figure 3) shows two stages: PWV values lower than 2 mm and PWV values more than 2 mm.

In the following sections we analyze the synoptic patterns that explain this PWV behavior.

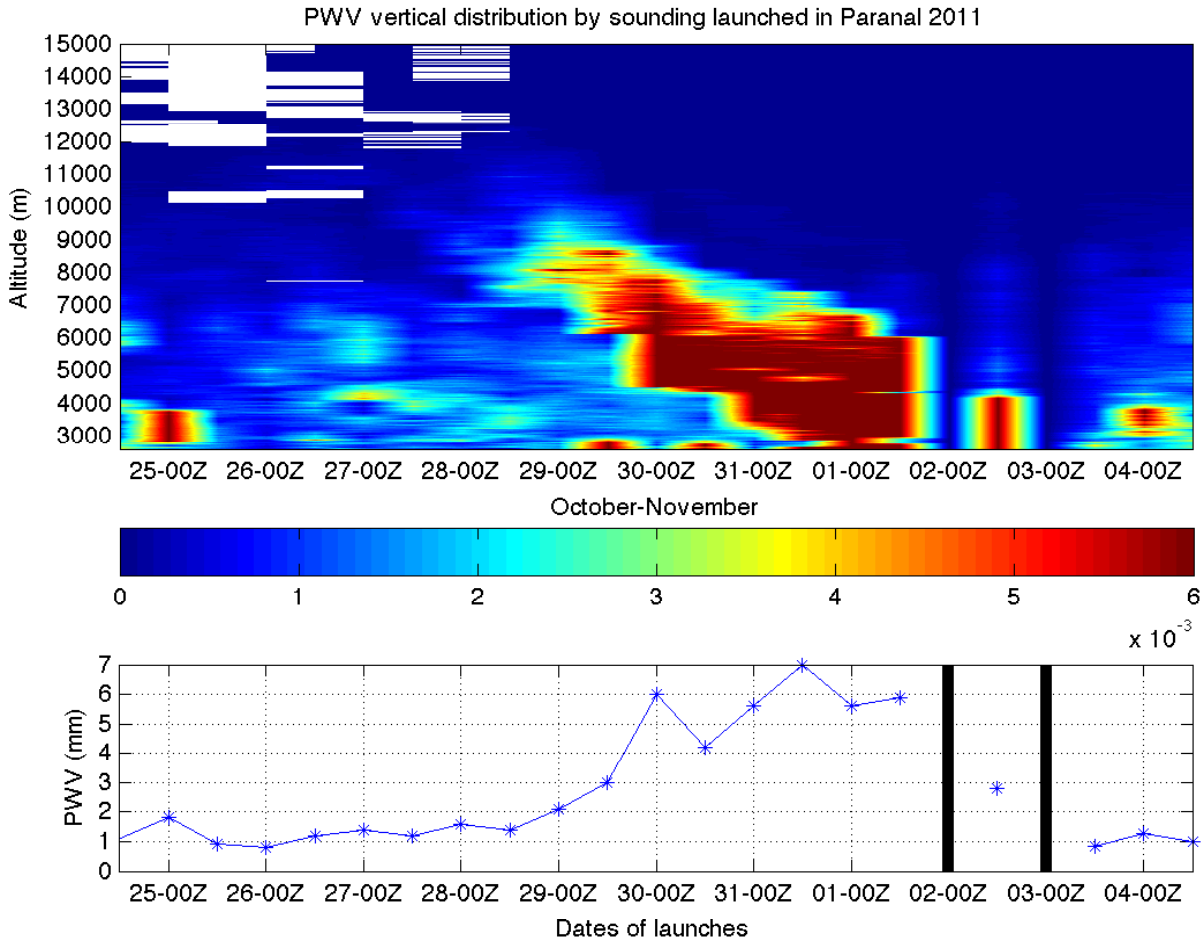

Figure 3: Vertical distribution of PWV measurement by radiosonde campaign in Paranal 2011 (Top). Total PWV measured by radiosonde (Bottom). The black vertical lines represent no launches.

4.2.1 Low PWV values

Between October 24th - 12UTC and 28th - 12UTC the PWV values measured by radiosondes were lower than 2 mm. In this period a dry and stable atmosphere influenced the skies of Paranal (Figure 3), this condition were related to the Anticyclonic Predominance (AP). This climate-meteorological pattern controls the weather condition the majority of the time in the Paranal zone. Figure 4 shows this typically condition at 700 hPa near of the Paranal altitude between 24th-12UTC and 25th-12UTC. Red colors are related to atmospheric stability and is dominant near of Paranal zone.

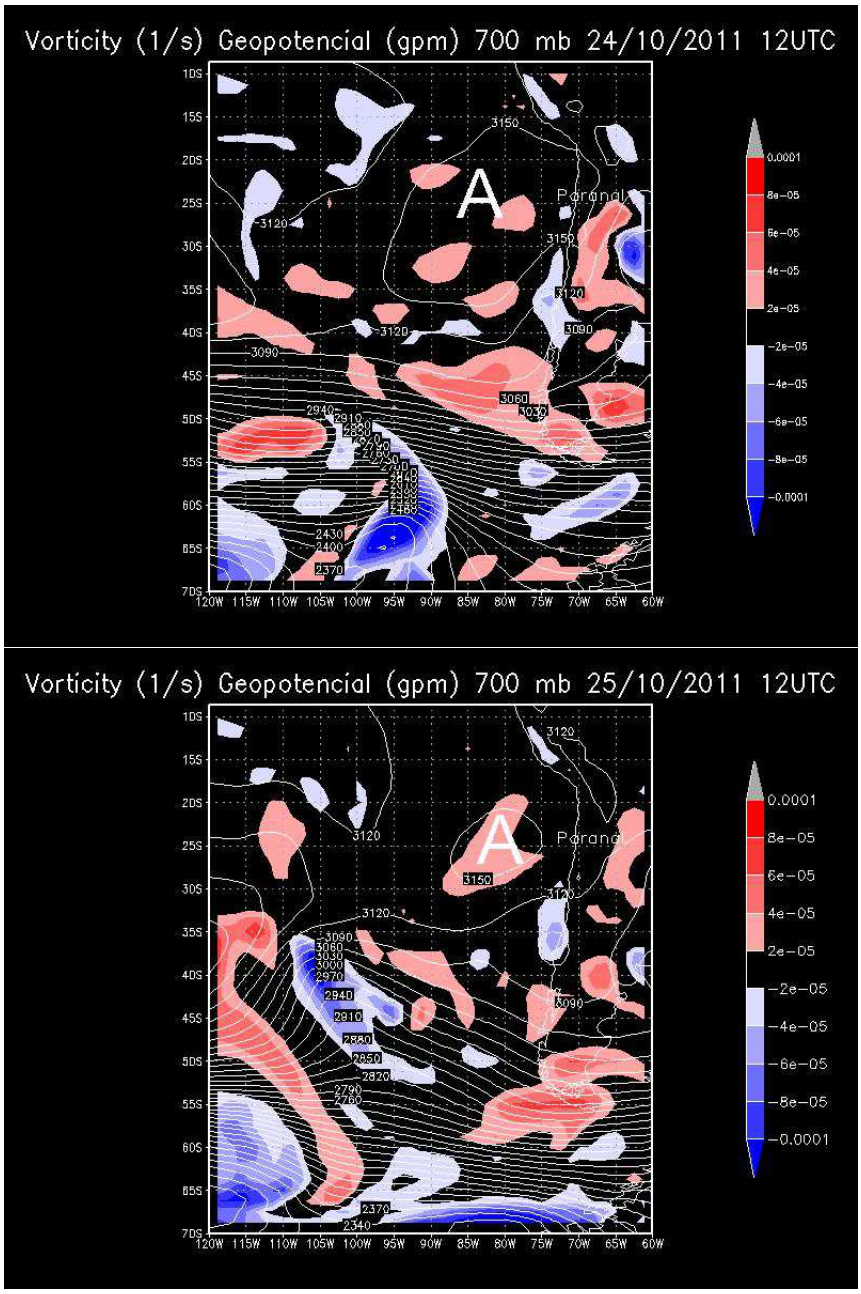

Figure 4: Vorticity (shadows) and geopotential height (contour) in 700 hPa. *Source: GFS global model.*

In the first part of the radiosonde campaign we found a PWV case (1.8 mm) over a short time interval, which will be studies in the following section.

25th October case

Figure 3 shows layers of humidity (PWV = 1.8 mm) near the surface on October 25th 00UTC. This case responds to an air advection from the North-NorthEast (Figure 5) between Paranal surface and 4000 m.a.s.l. These conditions are typical for the formation of a Coastal Low (CL), where the south part of the CL present an East component in the wind circulation (Low pressure is associate with cyclonic circulation). In the transition between the AP and CL the local pressure change from high to low values. This condition is clear in Figure 6 where the pressure changes between October 24th and 27th.

The surface chart (Figure 7) shows the evolution in the formation of the CL, and the transition of the AP to CL is clear in Figure 7. These synoptic situations suggest that the air mass with humidity from the warm tropical zone arrive to Paranal, but this does not happen in all cases, just when the center of the AP is located Southern of the normal condition and also when the CL is stronger.

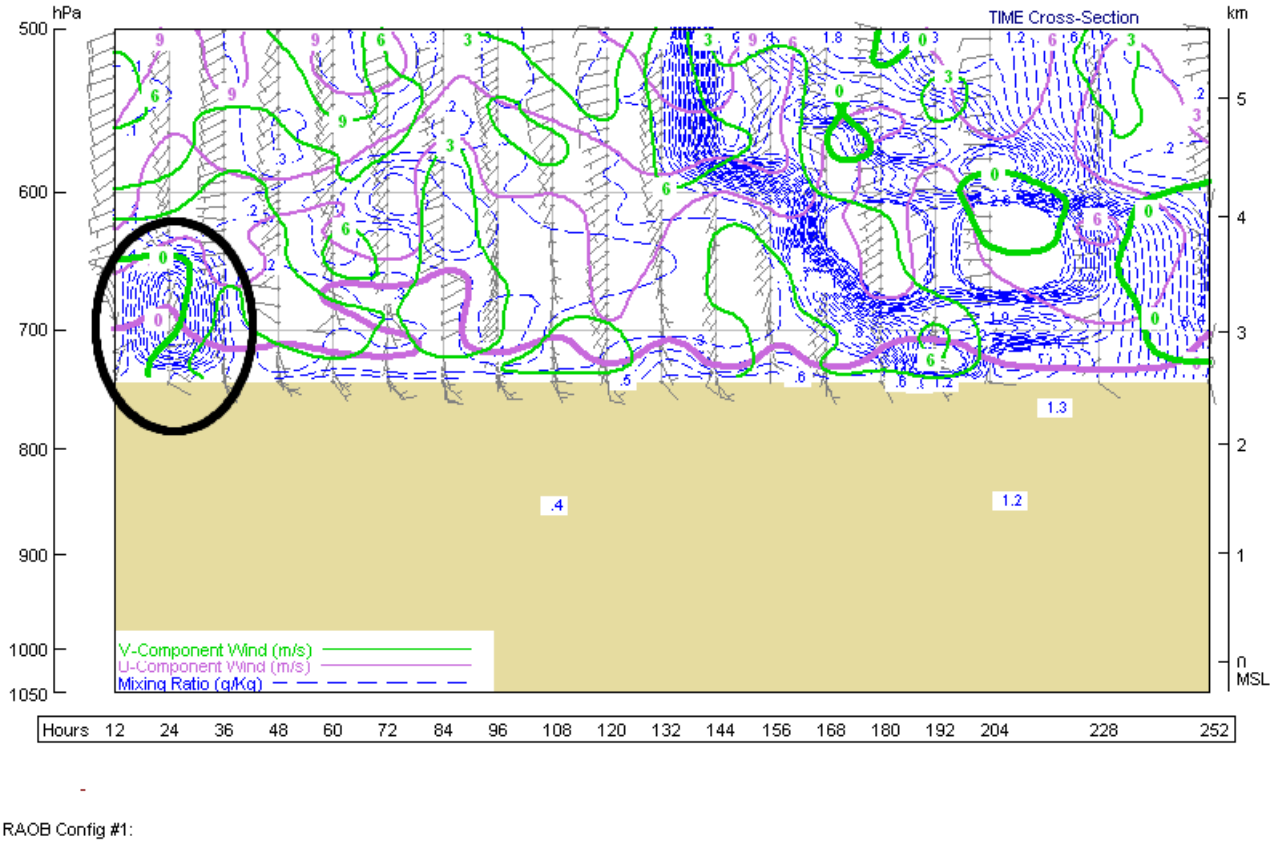

Figure 5: Analysis of the vertical profiles radiosonde campaign. Black circle shows the humidity (blue dash line) and component u (meridional in red) and v (latitudinal in green) of the wind. Values of wind<0 represent wind form North-East in the South Hemisphere. Valid for 25/10/2011 case.

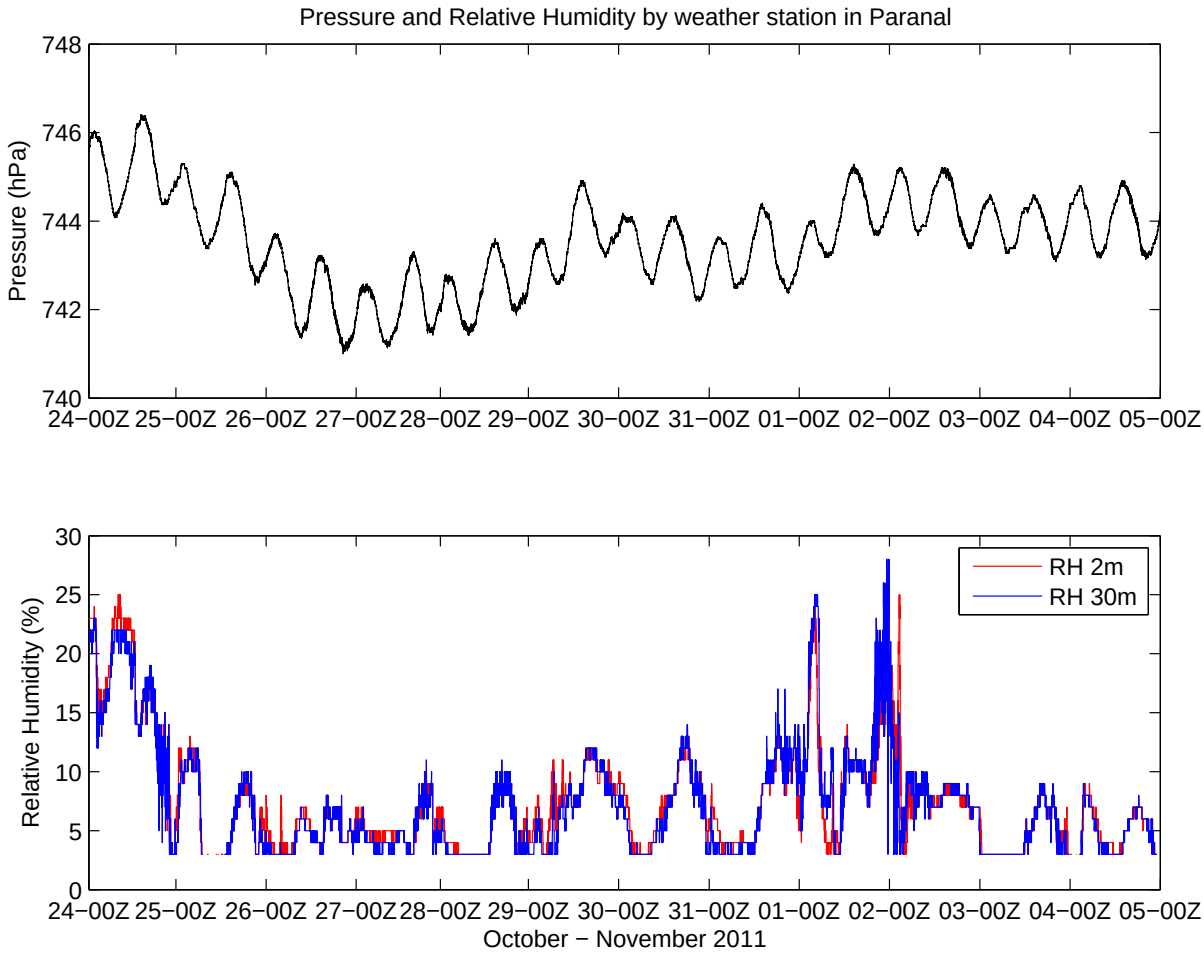

Figure 6: Local weather variables on Paranal during radiosonde campaign period. Top: Pressure at Paranal level. Bottom: Relative Humidity. Source: Paranal weather station.

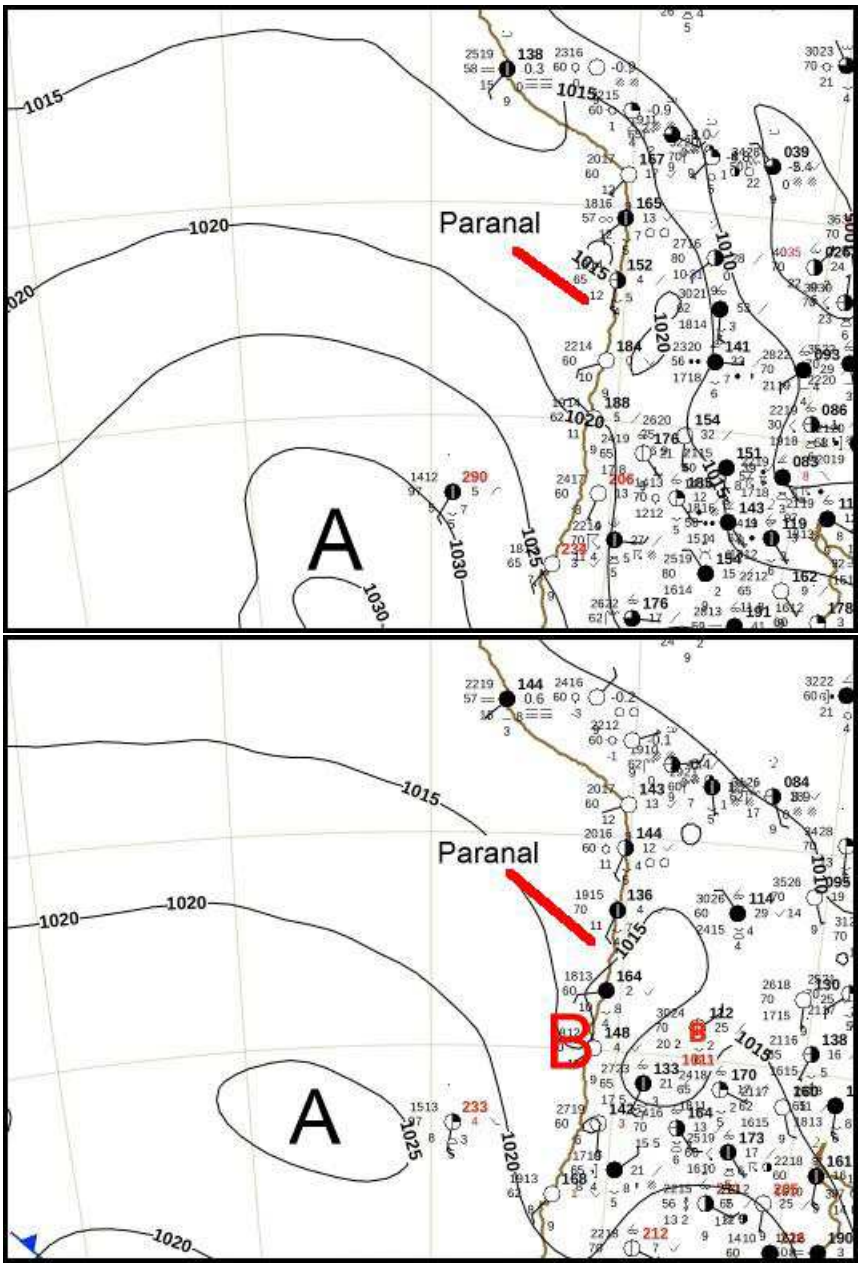

Figure 7: Pressure surface chart valid for 25/10/2011 at 00UTC and 26/10/2011 at 00UTC. A= Anticyclonic; B=Low Coastal. *Source: www.meteo.gob.cl*

4.2.2 High PWV values

Between October 29th to November 2nd a high case of PWV was registered by the radiosondes. This event was responsible for an advection of humidity from the Altiplanic Winter (AW), formed between October 26th to 27th (Figure 9). Part of this event was dispersed to South, where the subtropical Jet Stream (JS) takes its humidity and translates the air mass to South-East in the direction of the Paranal zone. The air mass has low velocity to South-East and it was push down by the JS, then it was compressed to the ground when the AP started to dominate (Figure 10). The JS put a top for this air mass and the highest wind intensity is near the Paranal zone, bringing clouds at high and middle levels between 28th and 29th October (Figure 8). Figure 11 shows the presence of the JS in 250 hPa and the most intensity of the wind is near of the Paranal.

In the middle atmosphere at pressure level of 500 hPa (figure 12), the anticyclonic predominance and the air motion from the west helps the wet air mass remain in a stable atmosphere, so it requires a longer time for dissipation.

Finally the humidity arrived to the surface of Paranal between November 1st and 2nd (Relative Humidity Figure 6) where it was dissipated and the atmospheric stability dominates until the end part of radiosonde campaign.

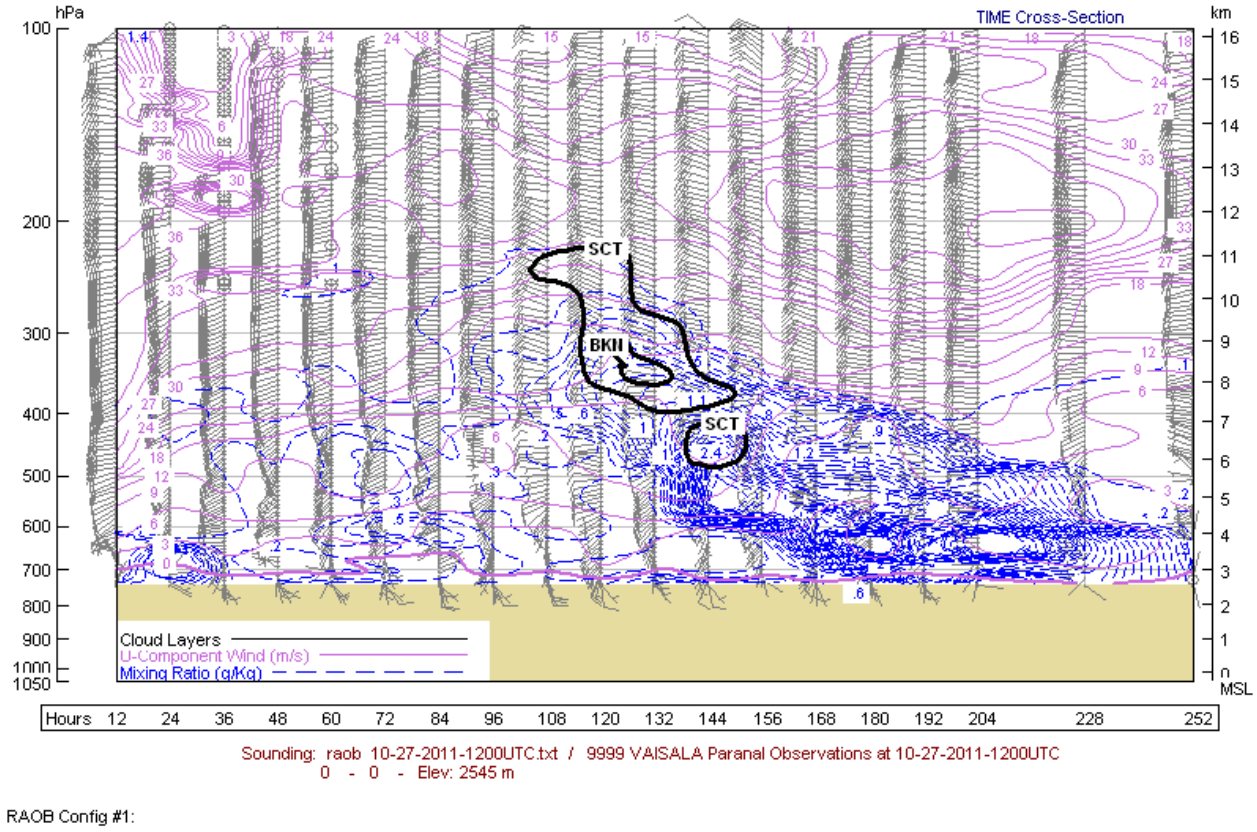

Figure 8: Time Cross-Section of the radiosonde campaign.

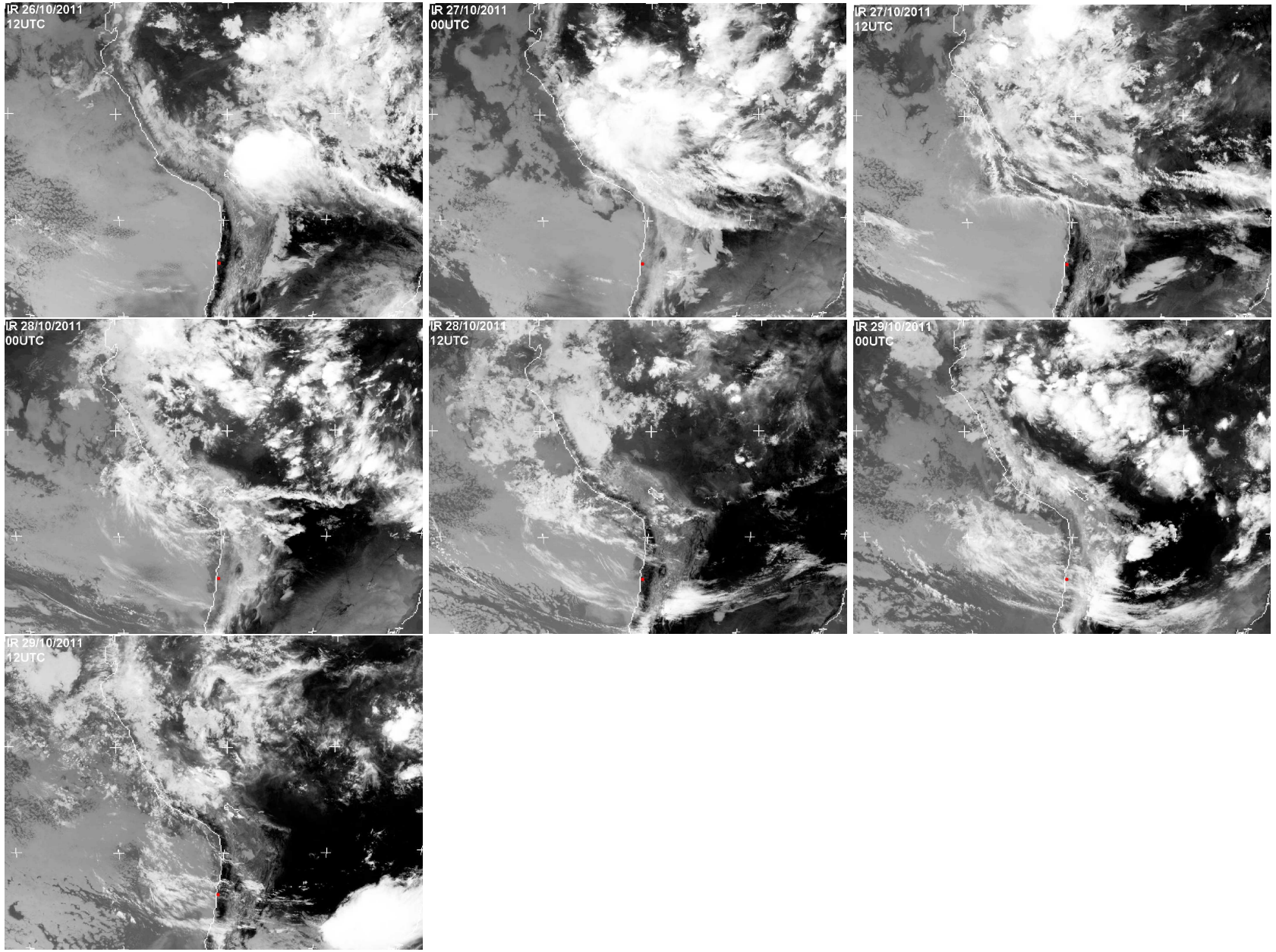

Figure 9: Altiplanic Winter case in infrared satellite images. Between 26/10/2011 to 29/10/2011. Paranal zone is marked with red point. *Source GOES-13*.

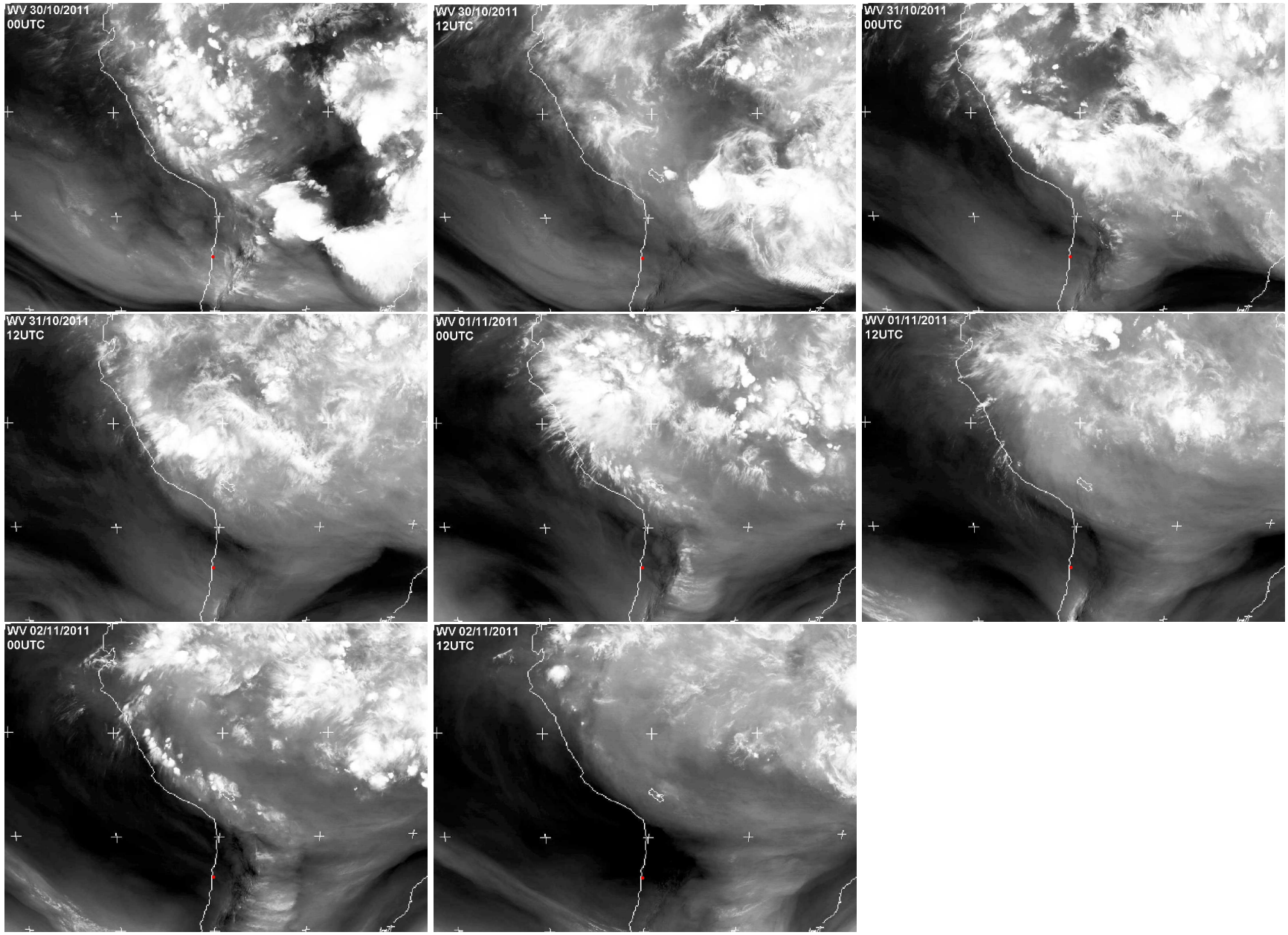

Figure 10: Humidity that arrived to Paranal after the AW case in water vapor satellite images. Between 30/10/2011 to 02/11/2011. Paranal zone is marked with red point. *Source GOES-13.*

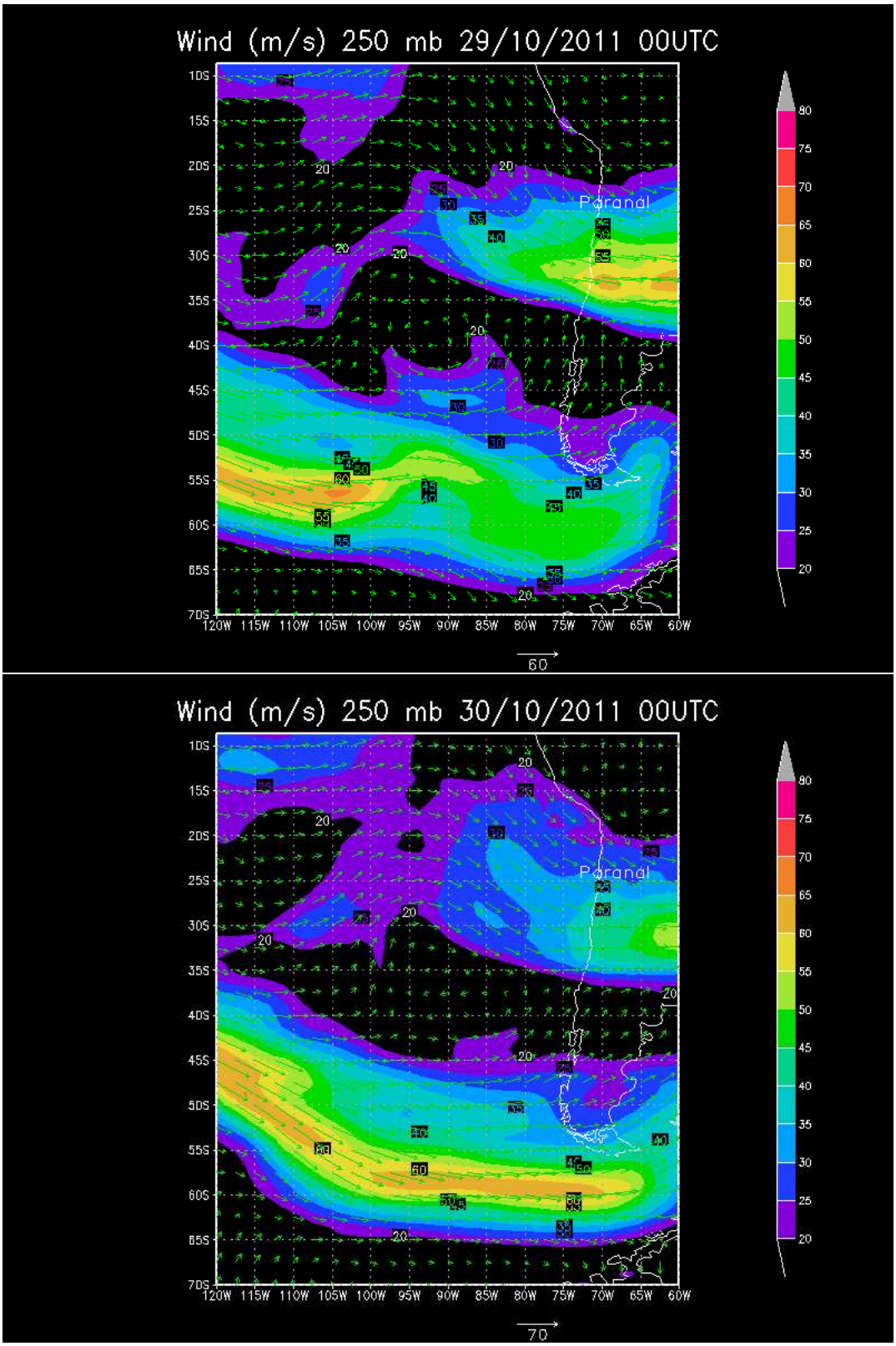

Figure 11: Vector and intensity of wind charts in 250 hPa. *Source: GFS global model.*

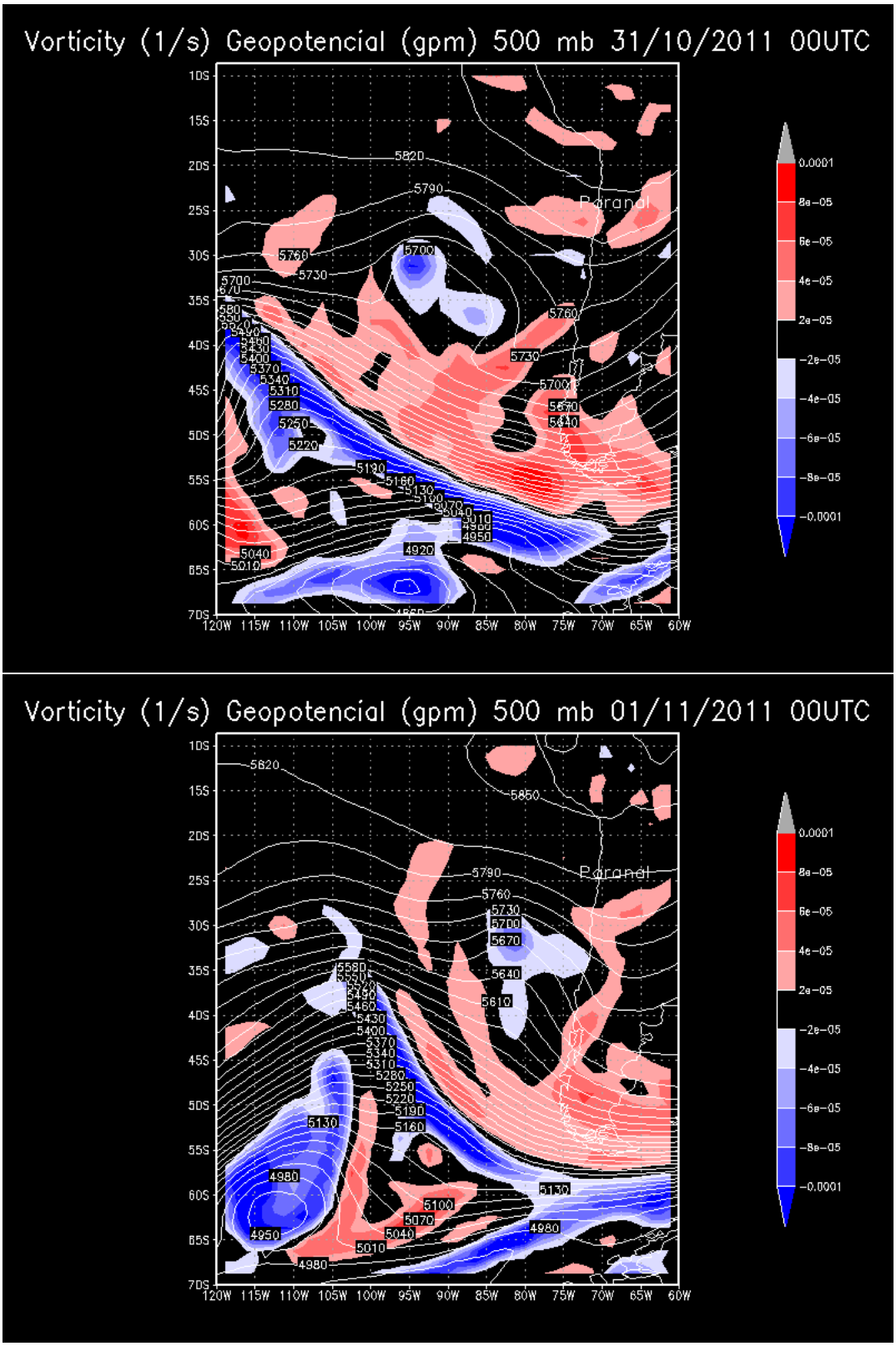

Figure 12: Vorticity (shadows) and geopotential height (contour) in 500 hPa. *Source: GFS global model.*

5 Atmospheric simulations

For the radiosonde campaign the AstroMeteorology group performed atmospheric simulations using the WRF[5] mesoscale meteorological code using high horizontal and vertical resolution. The WRF model was configured to the Paranal observatory using the following configuration:

Domain	Grid distance (Km)	Points West-East	Grid distance (Km)	Points South-North	Area (Km^2)	Vertical levels
1	27	70	27	53	1890 x 1431	50
2	9	82	9	73	738 x 657	50
3	3	97	3	97	291 x 291	50
4	1	67	1	67	67 x 67	50

Table 2: Domains selected for simulations with WRF for Paranal Observatory.

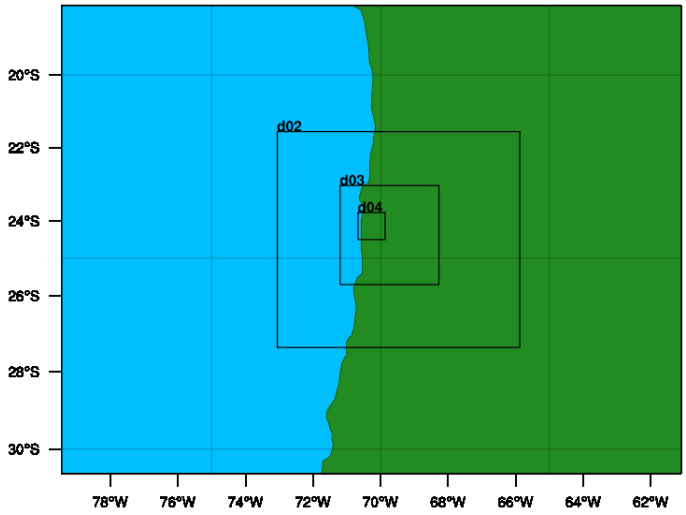

Figure 13: Domains distribution in WRF model. D4 on Paranal zone.

Currently, the AstroMeteorology group developed a project for ESO-Paranal with the objective to determine the best set of parameterizations of the WRF model and find the best configurations to simulate and forecast the weather conditions in a realistic form. The first result of this project showed that the two configurations showed in table 3 are the best ones, where is relevant the planetary boundary layer (PBL) parameterization. Based on this results we used the Mellor-Yamada-Janjic (MYJ) PBL [Janjic, 2002] in one configuration of the WRF model and also we used the Yensei-University (YSU) PBL [Hong et al., 2006] in the other configuration (Table 3). Both simulations will be compared with the radiosonde data in this section.

Name	Surface and boundary layer	Cumulus and Microphysics	Surface physics
MYJ	Mellor-Yamada-Janjic PBL Mellor and Yamada, 1982 and Janjic, 1990, 1996, 2002	WSM3 Hong et al, 2004	Noah Land-Surface model
YSU	Yonsei University PBL. Hong et al, 2006	WSM3 Hong et al, 2004	Thermal diffusion scheme

Table 3: Configurations used in WRF model.

[5]Weather Research and Forecast model: http://www.wrf-model.org/index.php

5.1 Synoptic analysis

At a synoptical scale (100 to 10 km and days to hours) radiosonde data are a very valuable, because they show all the meteorological process in the troposphere. The radiosonde sensors are the only instrument that can measure with high vertical and temporal resolution and for our case allows us to compare it with the WRF simulations, providing important information about the applications of the model in the weather forecast and some special astro-meteorological variables.

The comparison of the PWV vertical distribution between the radiosonde and the two WRF configurations show good agreement, Figures 14 and 15 show the lowest and highest PWV episodes with the same distribution as Figure 3. Although the vertical distribution of PWV is almost the same in both cases, the value of PWV calculated in the vertical column shows a difference. Both cases underestimated the PWV values in the highest case between October 29th and November 2nd. The maximum value of PWV measured by radiosonde was 7 mm but in the simulations was no more than 3.5 mm. These difference suggest a large error in numeric comparisons, but not from a synoptic point view because in both simulations the values of PWV follow the trend of the low and highest cases.

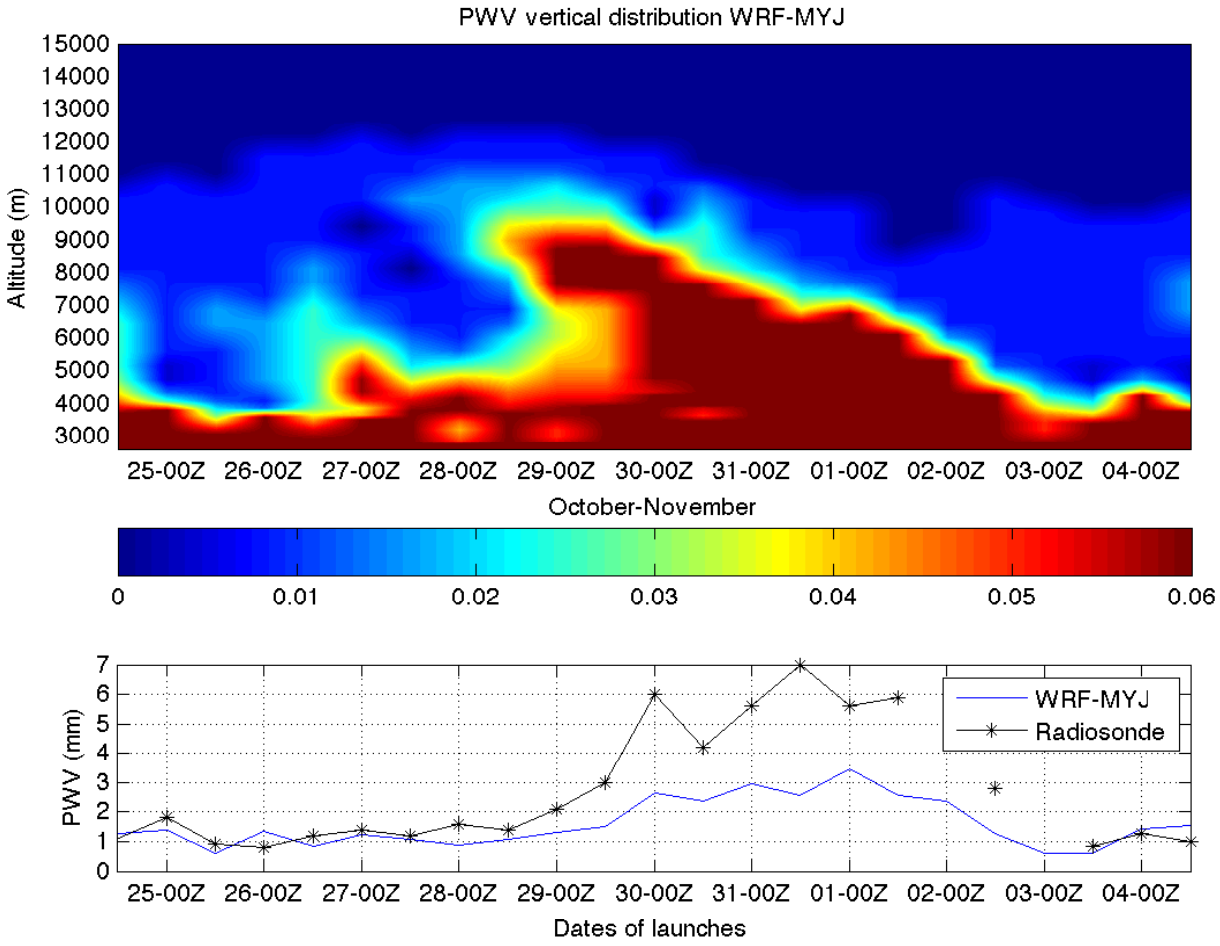

Figure 14: Vertical distribution of PWV simulated with WRF-MYJ configuration in Paranal 2011 (Top). Total PWV simulated by WRF-MYJ at 00UTC y 12UTC (blue) and measured by radiosonde (black) (Bottom).

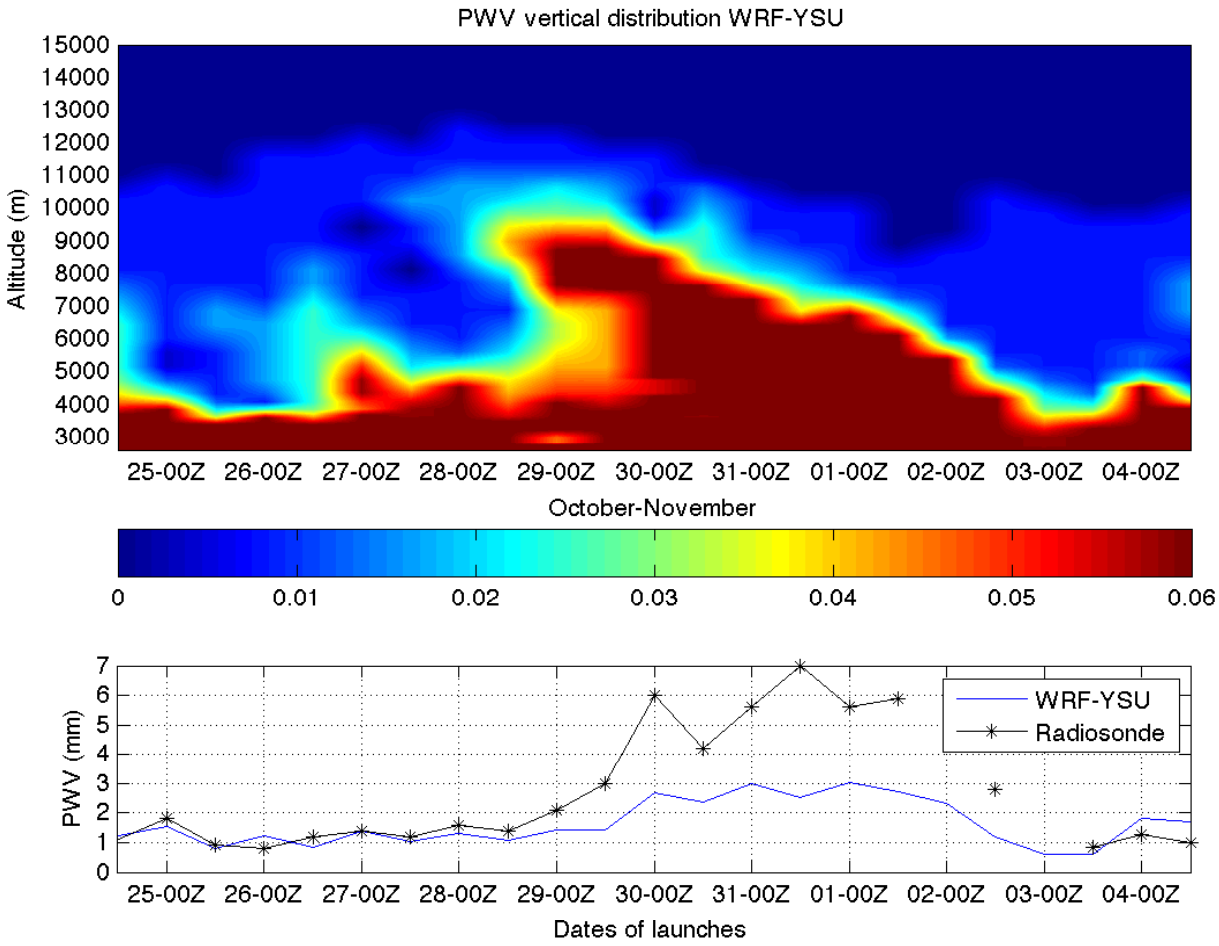

Figure 15: Vertical distribution of PWV simulated with WRF-YSU configuration in Paranal 2011 (Top). Total PWV simulated by WRF-YSU at 00UTC and 12UTC (blue) and measured by radiosonde (black) (Bottom).

5.2 PWV forecast

The initialization of the WRF simulation were 6 hours before of each radiosonde launch at 00 UTC. Table 4 shows the forecast hours related to 00 and 12 UTC hours (hours of radiosondes launches).

Figures 14 and 15 show a good agreement between the radiosonde and WRF simulations for the PWV's low case, but not for the highest PWV case because the WRF underestimate the maximum values over 3.5 mm. These figures show the simulations at 00UTC and 12UTC valid for 06 and 18 hrs of forecast each day.

Also we evaluate the forecast of the simulations until 66 hrs for every run between October 22th to November 03th 2011 (Table 4). The data show that the first 18 hrs of the model forecast are close to the observation but the following hours are close to the observation but afterwards the PWV values show larger dispersion. For the low PWV values cases (between 24th to 29th October) both WRF configurations are close of the radiosonde (Figures 16 and 17 at top) but in the high PWV values case the dispersion is large (Figures 16 and 17 at bottom). The WRF-MYJ shows variability on the forecast in the high PWV cases (Figure 16), but the WRF-YSU forecast of PWV started closer to the observations, but the agreement decrease on the time with larger errors (Figure 17). The simulations demonstrate that the performance of the WRF forecast is much better for low cases of PWV (PWV $<$ 2.5 mm) but in high cases of PWV (3 mm $<$ PWV $<$ 7 mm) the error is large because the WRF forecast were no more that 3.5 mm. However, the WRF follow the trends for lower and higher values of PWV measured, and in these case, the model showed the event where the PWV were higher by synoptic phenomena (AW-JS). The WRF could be a very good estimator for these kind of PWV events.

Run 18Z Day -1	Day 1		Day 2		Day 3	
UTC	00 UTC	12 UTC	00 UTC	12 UTC	00 UTC	12 UTC
Forecast	06	18	30	42	54	66

Table 4: Forecast setting of WRF model.

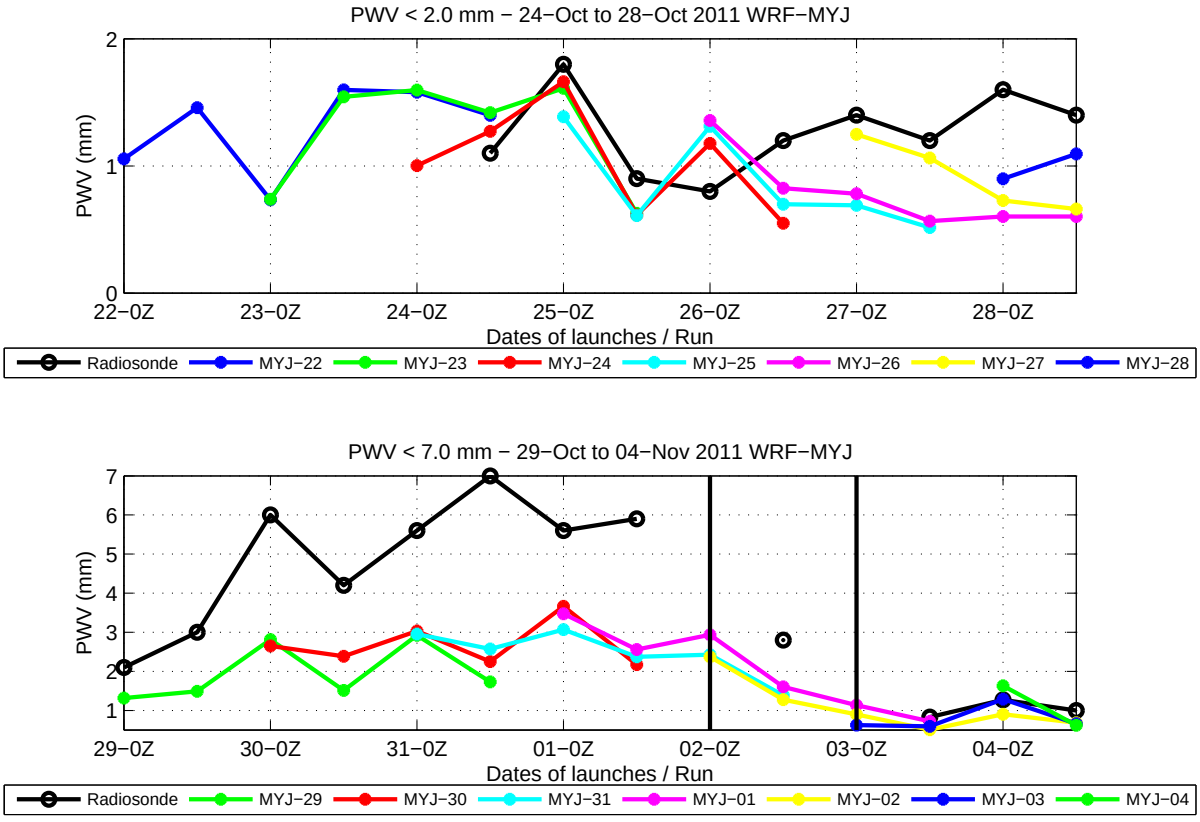

Figure 16: Daily WRF run. PWV forecast 06 to 66 hrs. WRF-MYJ. Top: Between 22-Oct to 28 Oct of 2011. Bottom: 29-Oct to 04-Nov 2011.

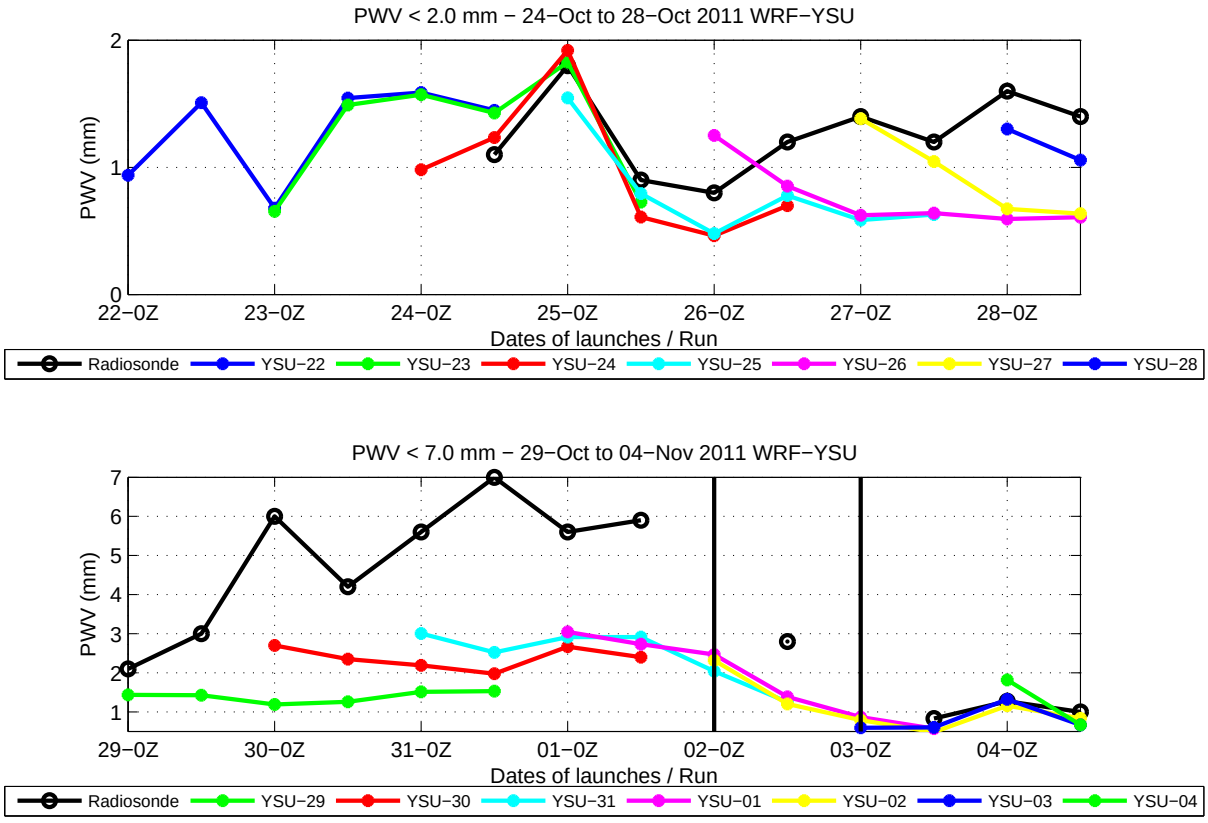

Figure 17: Daily WRF run. PWV forecast 06 to 66 hrs. WRF-YSU. Top: Between 22-Oct to 28 Oct of 2011. Bottom: 29-Oct to 04-Nov 2011.

The PWV simulated by WRF model were evaluated at 00 and 12 UTC (radiosonde launched), for the forecast hours showed in the table 4.

Hours	BIAS		RMSE		CORR	
	MYJ	YSU	MYJ	YSU	MYJ	YSU
06	-0.85	-0.78	1.47	1.50	0.93	0.95
18	-1.19	-1.17	1.87	1.86	0.91	0.89
30	-0.94	-1.25	1.52	2.00	0.93	0.68
42	-1.49	-1.51	2.09	2.11	0.91	0.84
54	-1.16	-1.41	1.89	2.22	0.67	0.56
66	-1.61	-1.59	2.27	2.30	0.84	0.77

Table 5: Statistics parameters (BIAS, RMSE & Corr) for the campaign of PWV measurements.

Figure 18 shows the time series of the values measured at 00 UTC (Radiosonde) and the values simulated by the two configurations (MYJ and YSU) at 06 (a), 30 (b) and 54 F (c). Both configurations of the WRF model underestimate the values of PWV, especially the high values measured by radiosondes. Figure 18 presents a similar behavior, but in Figures 18b and c the MYJ configuration is closer to the values measured by the radiosondes, particularly in the high values of PWV. Table 5 shows that the best correlations were by MYJ configurations at 06 and 30 F and also the lowest RMSE (1.5 mm).

Figure 19 shows the comparison of the values measured by radiosonde at 12 UTC and the simulated ones 18 (a), 42(b) and 66 F(c). Both configurations show an underestimation of the PWV, especially for high values of PWV measured by radiosonde. The error in this period were larger than the errors at 00 UTC (Table 5). MYJ and YSU configurations show the same values of RMSE at 18, 42 and 66 forecast hours respectively and also show high values in the correlations at the same hours (Table 5).

The larger errors were located near of the ground of Paranal, where the complex orography and the resolutions of boundary conditions of GFS/FNL global models lead to systematic errors in the simulations of the WRF model. Statistic techniques like a Kalman filter can help reduce the systematic errors. A Kalman filter was used

with excellent results by AstroMeteorology group [Doc 2] and could be a powerful tool to reduce systematic errors on WRF models.

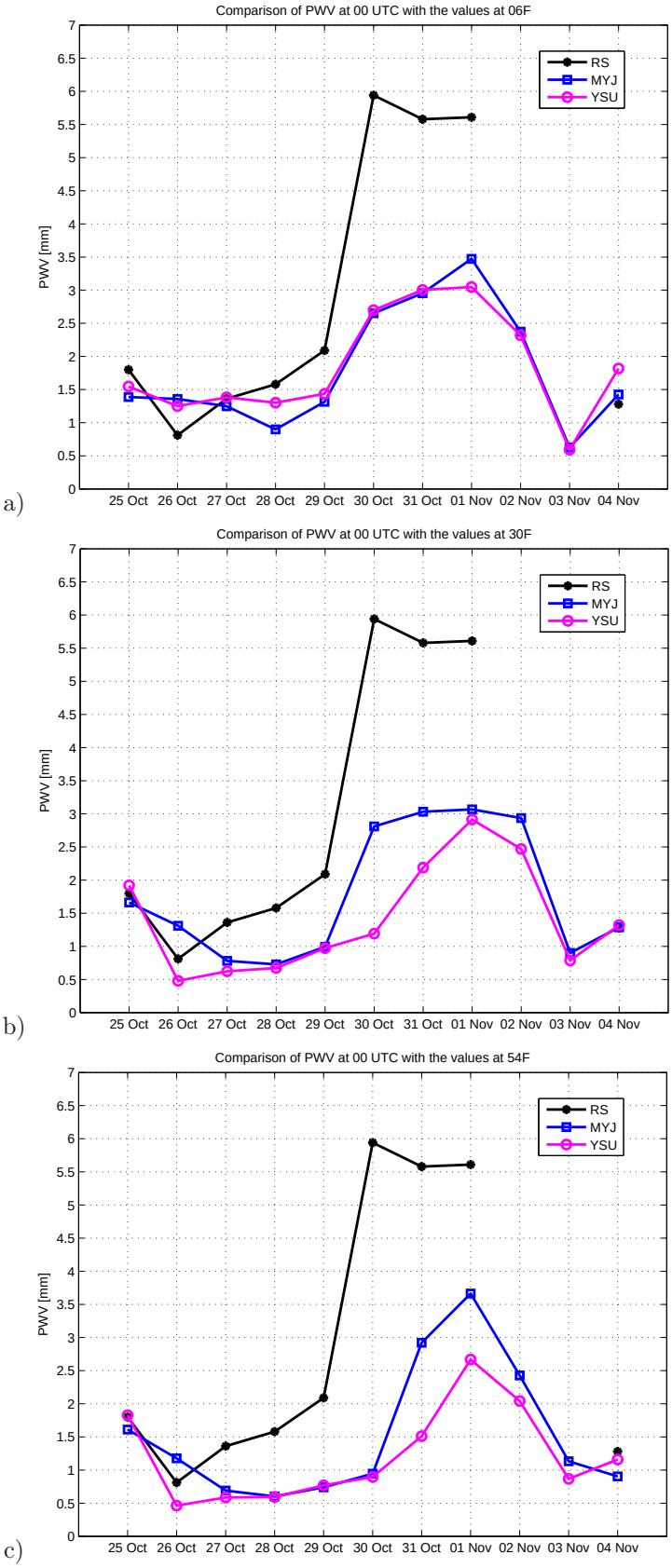

Figure 18: Comparison between PWV measured by the radiosonde (black line), NOAH configuration (blue line) and YSU configuration (magenta line) at a) 00 UTC and 06 F, b) 00 UTC and 30F and c)00 UTC and 54F.

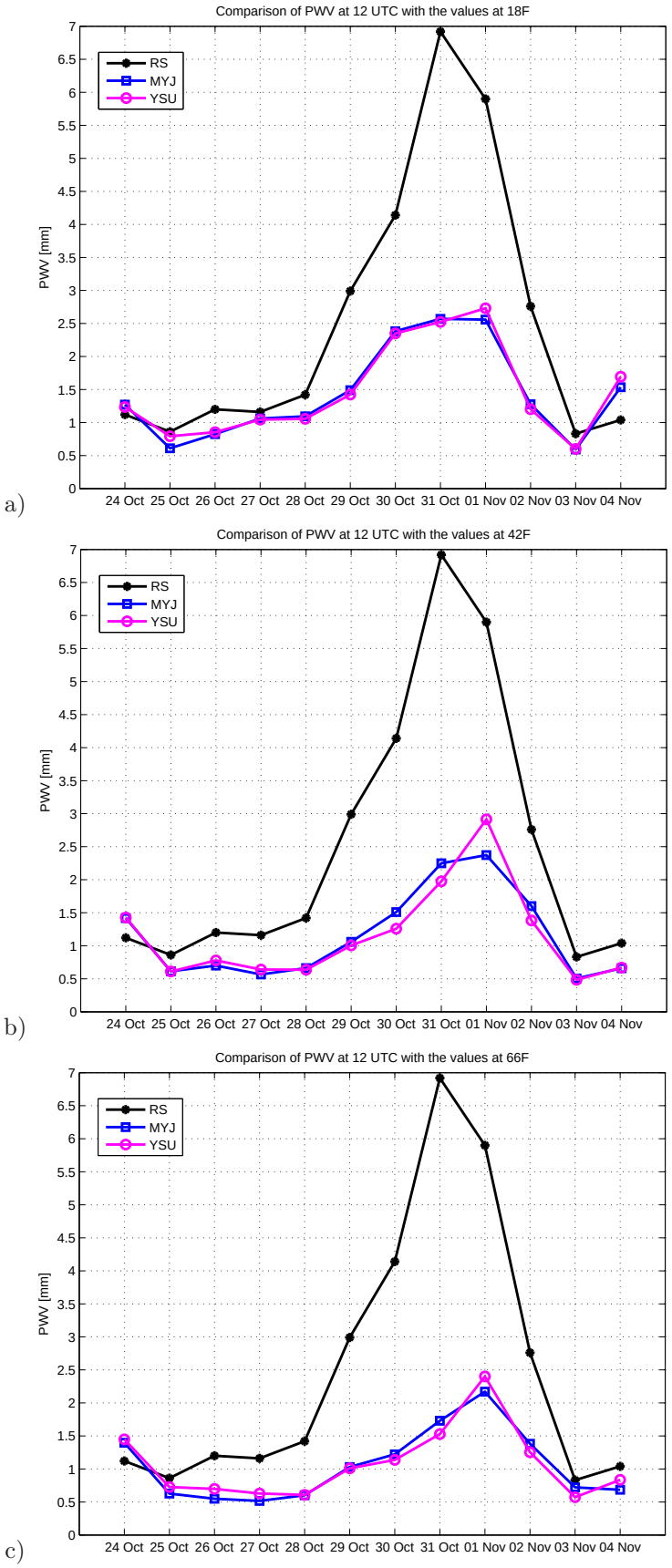

Figure 19: Comparison between PWV measured by the radiosonde (black line), NOAH configuration (blue line) and YSU configuration (magenta line) at a) 12 UTC and 18F, b) 12 UTC and 42F and c) 12 UTC and 66F.

5.3 Evaluation of Vertical Profiles

WRF vertical profiles were extracted from domain 4 (highest resolution ~1 Km) using a bilinear interpolation to select the point where the campaign launching took place. An average profile of 00 UTC and 12 UTC were calculated from radiosondes and from the WRF simulation for each forecast hours (Table 4). The meteorological variables evaluated were: temperature, relative humidity, water mixing ratio, speed and direction of wind.

5.3.1 Temperature

The temperature vertical profiles from the WRF model are similar to the profiles measured by the radiosondes at 00 and 12 UTC (Figure 20 and 21). In both hours the forecast mean profiles present an underestimation in the lower pressure levels (750 to 650 hPa). YSU configuration present the lowest errors in those levels (less than 1.5ºC) in the forecast of 00 UTC and the forecast of 12 UTC both configurations present the same behavior with a BIAS less than 2.5ºC. As for RMSE forecast profiles of 00 UTC, the errors are not more than 1.7ºC between 750 and 500 hPa, in the upper levels of pressure the error is less than a 1ºC, for YSU configuration (Figure 20c). In the 12 UTC hours comparison, both configurations present errors not more than 2.7ºC between 750 to 700 hPa and for the other levels of pressure the errors are less than 2ºC (Figure 21c).

5.3.2 Relative humidity

Relative humidity profiles (Appendix B: Figure 22 and 23) show an overestimation of the values of less than 15% in both configurations in low and high levels of pressure. In middle levels of pressure present an overestimation in the hours of 00 UTC ($<$ 9%, Appendix B: Figure 22b), but in the hours of 12 UTC the behavior of the configurations is almost the same as the measured data (Appendix B: Figure 23b. The low RMSE values were presented by both configurations at 12 UTC with a value of less than 15% between 750 to 400 hPa. At 00 UTC hour the RMSE values increase as the forecast hours increase, between 20% and 25% (Appendix B: Figure 22c). The biggest values of RMSE are shown in the upper level (app 300 hPa to 100 hPa) because the values are more than 25% in both configurations.

5.3.3 Mixing ratio

Vertical profile of mixing ratio values were used to calculate the PWV. In the vertical profile (Appendix B 24 and 25) both configurations of WRF model overestimate the values between 750 to 620 hPa at 00 UTC and 12 UTC forecast hours. YSU configuration presents the lowest BIAS ($<$ 0.7 mm) and RMSE ($<$ 1.3 mm) at 30 and 54 forecast hours.

Between 600 to 400 hPa both configurations underestimate the values of mixing ratio but less than 0.5 mm and RMSE less than 1 mm (1.3 mm) in the forecast of 00 UTC and 12 UTC. In upper pressure levels both configurations behave the same way as the data measured by the radiosondes.

5.3.4 Wind speed

For vertical profiles of wind speed (Appendix B: Figures 26 and 27), both configuration of the WRF model present the same tendency as the measured data by the radiosondes at 00 and 12 UTC forecast hours. Both configurations of the WRF model overestimated the values but not more than 2.5 m/s in the low pressure levels and less than 5 m/s in upper pressure levels. The RMSE (Appendix B: Figure 26c and 27c) the values were below 4 m/s but in the upper levels of pressure, in average, can be less than 5.5 m/s.

5.3.5 Wind direction

Both configurations of the WRF model show good agreement with wind direction for pressure levels higher from 500 hPa with RMSE less than 14º in both hours under study (00 and 12 UTC; Appendix B: figures 28 and 29). For the levels below than 700 hPa both configurations presented an underestimation of no more than 60º at 00 UTC and no more than 30º at 12 UTC forecast hours. The highest RMSE values were presented in the lowest levels of pressure in both hours, but the best results were presented by YSU configuration at 30 and 54 forecast hour (between 30º to 75º). At 12 UTC forecast hour the RMSE values were between 30º to 105º.

In summary both configurations had similar performance in the vertical profile, but near the ground the YSU shows better agreement.

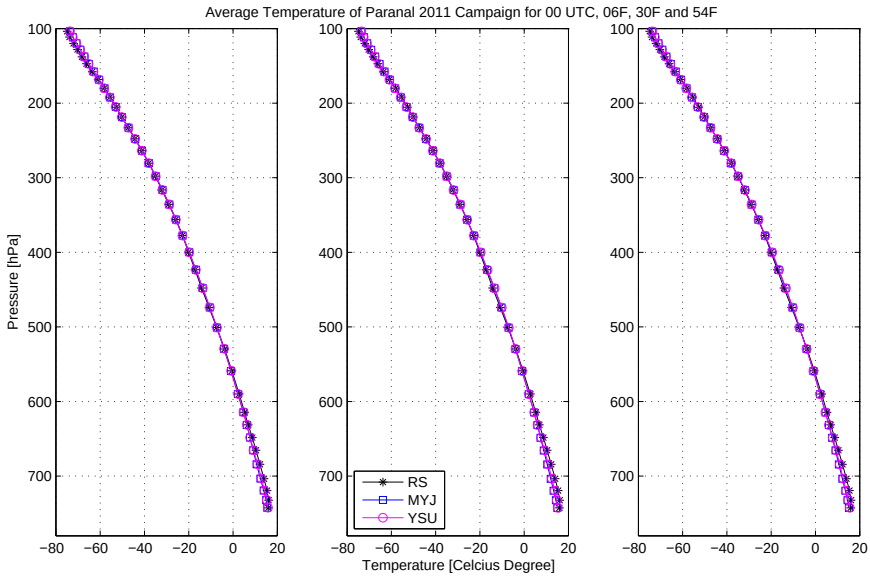

a)

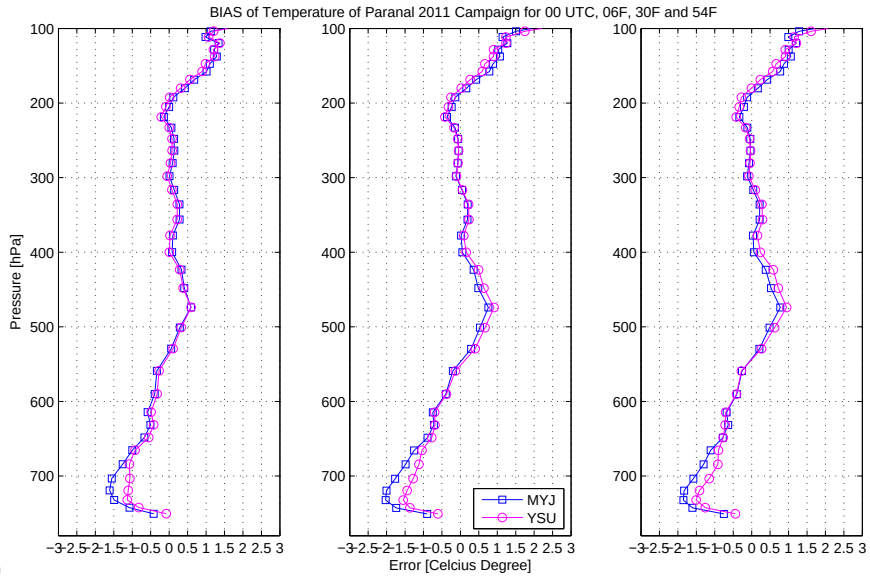

b)

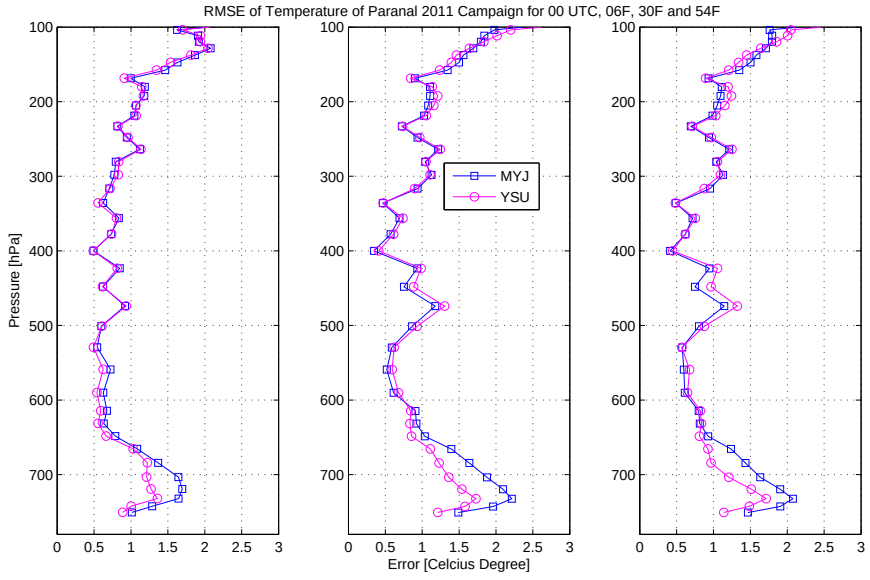

c)

Figure 20: a) Mean vertical profiles of temperature for radiosondes (black line), MYJ configuration (blue line) and YSU configuration (magenta line), b) vertical profile of BIAS and c) vertical profile of RMSE during the Paranal Campaign 2011.

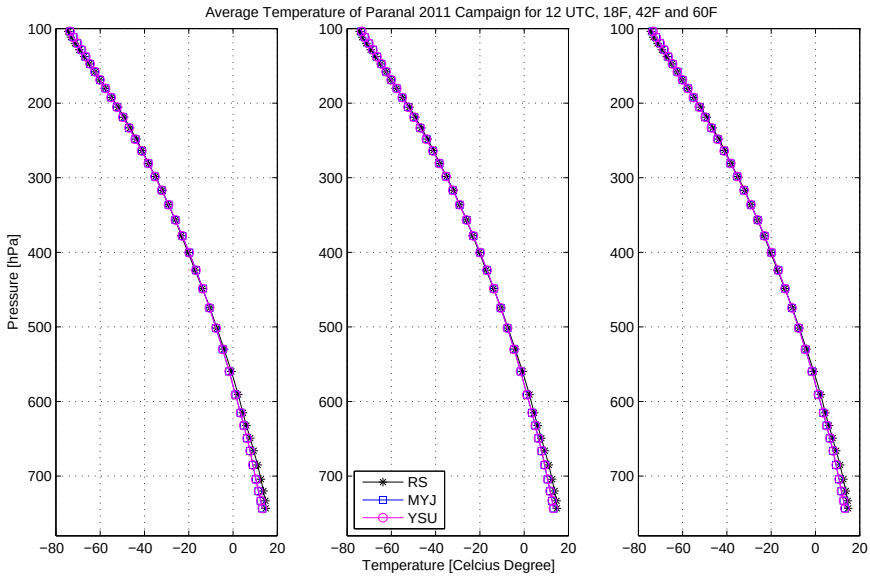

a)

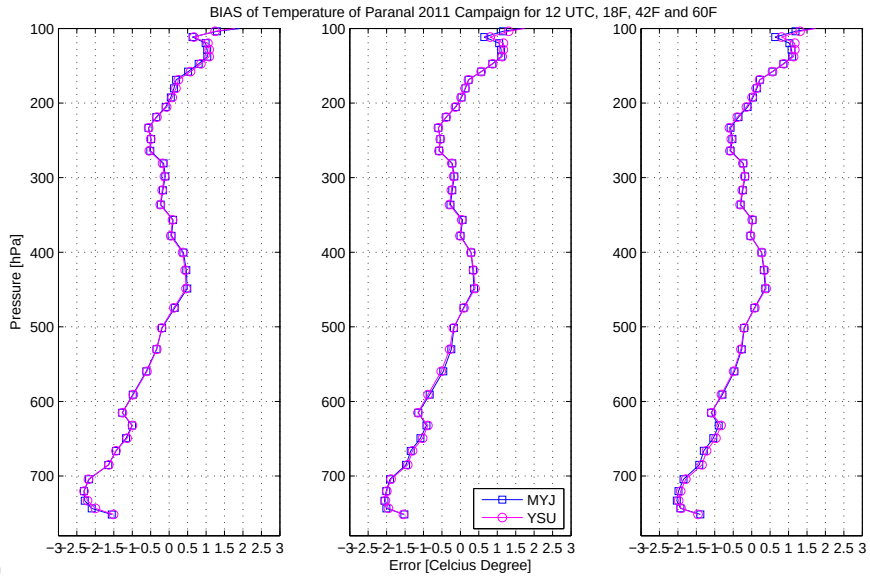

b)

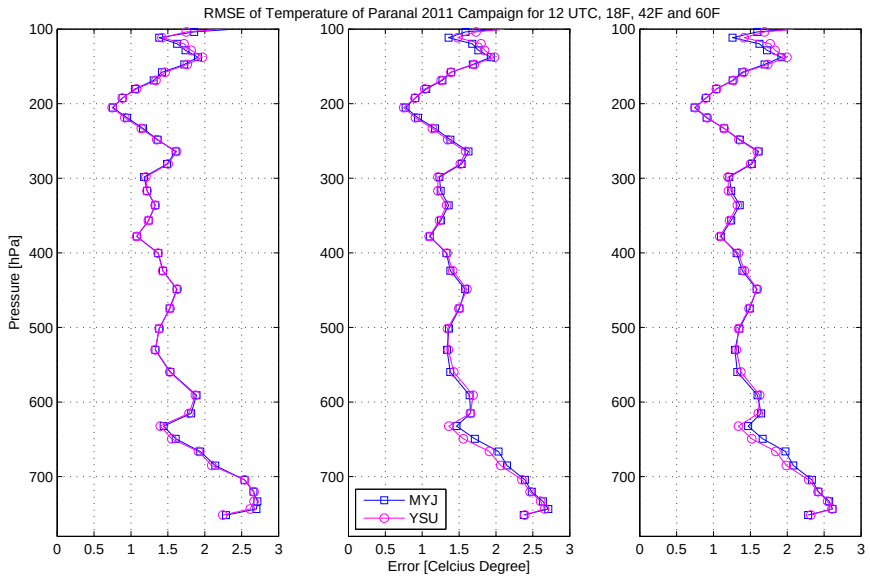

c)

Figure 21: a) Mean vertical profiles of temperature for radiosondes (black line), MYJ configuration (blue line) and YSU configuration (magenta line), b) vertical profile of BIAS and c) vertical profile of RMSE during the Paranal Campaign 2011.

6 Conclusions

The AstroMeteorology group participated in a project conduced by ESO in order to upgrade VISIR instrument in Paranal Observatory. Our group was in charge of the radiosonde launching and collection, reduction and delivery the data. In addition, we performed a meteorological analysis that involved numerical meteorological simulations using the WRF mesoscale model and compared it with the PWV values and standard meteorological data collected by the radiosonde campaign.

In the data measured by the radiosonde we found two stages of PWV values (Figure 3): low cases with PWV values less than 2mm and high cases of PWV with values larger than 2 mm with a maximum of 7mm. The meteorologic study showed a very good agreement between the synoptic patterns and the PWV values. In the first part of campaign, the Anticyclonic Predominance was controlled by low values of the PWV, associated to atmospheric stability, wind direction from the west and dry condition in almost all levels over Paranal site (Section 3.2.1). The analysis shows that in Anticyclonic Predominance condition a small layer of humidity affected to Paranal. This happened when the Costal Low was in formation in the west side of the Paranal over the coast. This synoptic pattern provoked cyclonic circulation, and the first day of formation (October 25th) an NorthEast wind affected the surface of Paranal with humidity from the tropical wet zone. This case happened the October 25th and it was explained in the section 3.2.1.

The second stage of the PWV values respond to a case of the advection of the humidity from the Altiplanic Winter. Part of the humidity from Altiplanic Winter was advected by the Jet Stream, which pushed down the air mass and then arrived to Paranal zone. The Altiplanic Winter formation was between October 26th and 27th but the humidity had an affect between October 28th to November 2nd. Both episodes were analyzed using satellite images form GOES (Figures 9 and 10). But considering the cases analyzed by radiosonde, satellite images and weather station; the following question arises: Could this be forecast? The answer is YES. We show that at synoptic and local scale, the cases of low and high PWV values can be forecast using a global model such as GFS and/or a mesoscale model such as WRF. The general circulation in synoptic scale can be contrasted perfectly using satellite images and a global model GFS, and it provides important tools that can monitor the evolution of these events and can forecast them. A powerful tool is the WRF model which demonstrated at the local scale that the distributions of PWV simulated (Figures 14 and 15) were very close of the PWV measured by radiosonde (Figure 3). Given the tendency for lowest and highest values of PWV cases, the WRF was very good estimator, because the model responded at events where the PWV were high in many consecutive days by the advection by synoptic phenomena (AW-JS). So, the WRF could be a very good estimator for these kind of PWV events.

PWV forecast evaluation from the WRF model shows that MYJ and YSU configurations underestimate the high case of PWV measured by radiosonde, but performs better in the forecast of the low values of PWV measured by radiosonde. The lowest errors were presented at the forecast at 00 UTC at 06 and 30 forecast hours by MYJ configuration (1.5 mm) with a correlation of 0.9. When considering the validation at 12 UTC forecast hour, both configurations (MYJ and YSU) were similar but with larger errors at 00 UTC. This was because the maximum values of PWV were measured at 12 UTC hour and the model could not adequately forecast well the values of PWV (error larger than 3.5 mm).

In regards to the validation of the vertical profiles from the two configurations of the WRF model (MYJ and YSU), the best performance was presented by YSU at 00 UTC forecast hour. The performance of both configurations present almost the same results at 12 UTC forecast hour. The best agreement of the vertical profile in both configurations of the WRF model were for the temperature, speed and direction of the wind. The mixing ratio is mostly overestimated in the levels near to the surface and the levels related to middle atmosphere the values are underestimated in both configurations. The simulation of relative humidity were overestimated in the upper levels.

Finally we demonstrate that the synoptic analysis could explain the episodes of the PWV in Paranal, and the use of the WRF mesoscale model is a powerful tool to forecast the standard and astro-meteorological variables in Paranal zone.

Acknowledgment

The AstroMeteorology group thank to the VISIR update project SOW-ESO to financial support of the radiosonde campaign and this report. Also we thank to ESO-Paranal staff to bring us the material and logistic support on the radiosonde campaign. Finally we specially thank to Julio Navarrete for all the support and logistics that provided us.

References

[Doc 1] AstroMeteorology group, 2010: Project: Study of Precipitable Water Vapor (PWV) at Llano de Chajnantor, Final Report. ESO project.

[Doc 2] AstroMeteorology group, 2010: ADDENDUM: Measuring and forecasting PWV above La Silla, APEX and Paranal observatories. ESO project.

[Janjic, 1990] Janjic, Z. I., 1990: The step-mountain coordinate: physical package, Mon. Wea. Rev., 118, 1429–1443.

[Janjic, 1996] Janjic, Z. I., 1996: The surface layer in the NCEP Eta Model, Eleventh Conference on Numerical Weather Prediction, Norfolk, VA, 19–23 August; Amer. Meteor. Soc., Boston, MA, 354–355.

[Janjic, 2002] Janjic, Z. I., 2002: Nonsingular Implementation of the Mellor–Yamada Level 2.5 Scheme in the NCEP Meso model, NCEP Office Note, No. 437, 61 pp.

[Hong et al., 2004] Hong, S.-Y., J. Dudhia, and S.-H. Chen, 2004: A Revised Approach to Ice Microphysical Processes for the Bulk Parameterization of Clouds and Precipitation, Mon. Wea. Rev., 132, 103–120.

[Hong et al., 2006] Hong, S.-Y., and Y. Noh, and J. Dudhia, 2006: A new vertical diffusion package with an explicit treatment of entrainment processes. Mon. Wea. Rev., 134, 2318–2341.

[Mellor and Yamada, 1982] Mellor, G. L., and T. Yamada, 1982: Development of a turbulence closure model for geophysical fluid problems. Rev. Geophys. Space Phys., 20, 851–87

Appendix A:

Instrumentation

The radiosonde instrumentation was the same used in the campaigns developed in 2009 by AstroMeteorology group in La Silla, Paranal and Chajnantor ESO's sites. The Vaisala's equipment used were:

Vaisala Radiosonde RS92-SGP

This radiosonde model measures humidity, pressure, temperature and wind speed and direction. Each radiosonde have a GPS receiver for wind finding, a silicon pressure sensor, heated twin humidity sensor and a small fast temperature sensor.

Vaisala Sounding Processing Subsystem SPS311

A fully digital telemetry link is implemented between the Vaisala Radiosondes RS92-SGP and the Vaisala Sounding Processing Subsystem SPS311. The SPS311's data reception technology makes extensive use of the software-defined radio technology. The radio signal is converted to fully digital format at very early phase of signal transmission, which improves performance in comparison with conventional analog receivers[6].

[6] Åkerberg J.: State-of-the-art radiosonde telemetry, Eighth Symposium on Integrated Observing and Assimilation Systems for Atmosphere, Oceans and Land Surface, American Meteorological Society, 2004.

a)

b)

Ground Check Set GC25

This instrument check the functioning of the radiosonde, the sensors accuracy and set the frequency of the radiosonde (Figure a).

Vaisala Portable Antenna Set CG31

Is a mobile antenna configuration designed to be used with GPS wind finding systems in the field conditions (Figure b). The antenna set consists of Helix UHF antenna, GPS antenna and the Antenna Amplifier and Switch RAA111 on a tripod mount.

A PC with DigiCORA sounding software is needed. This software interconnects the Vaisala Sounding Processing Subsystem SPS311 (the Vaisala Portable Antenna Set CG31 is connected to this device) and the Ground Check Set GC25.

The steps made to launch all the radiosondes were the following:

1. Perform sounding preparation (calibrate the frequency, sensor and telemetry).
2. Prepare the balloon.
3. Connect the battery.
4. Launch the radiosonde.
5. Monitor the sounding with the DigiCora Sounding System.

Appendix B:

Figures of the Section 4.3: Evaluation of vertical profile

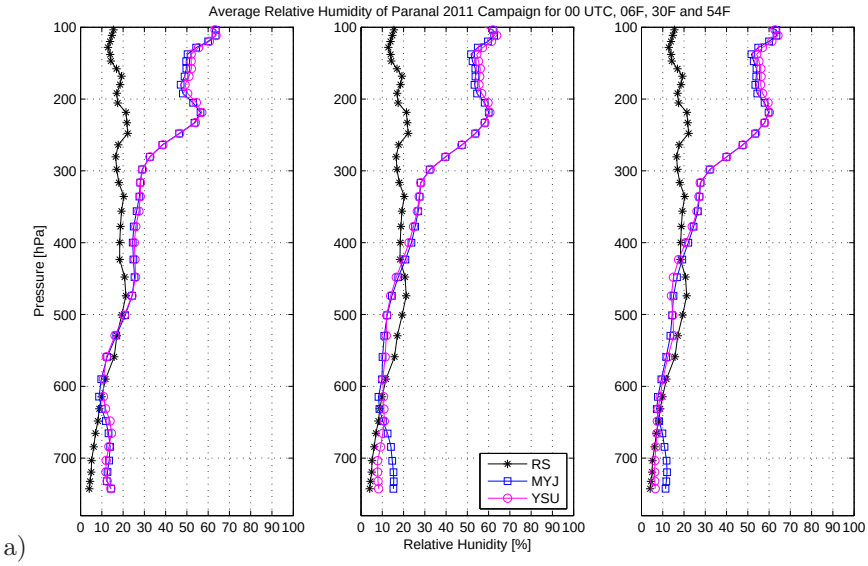

a)

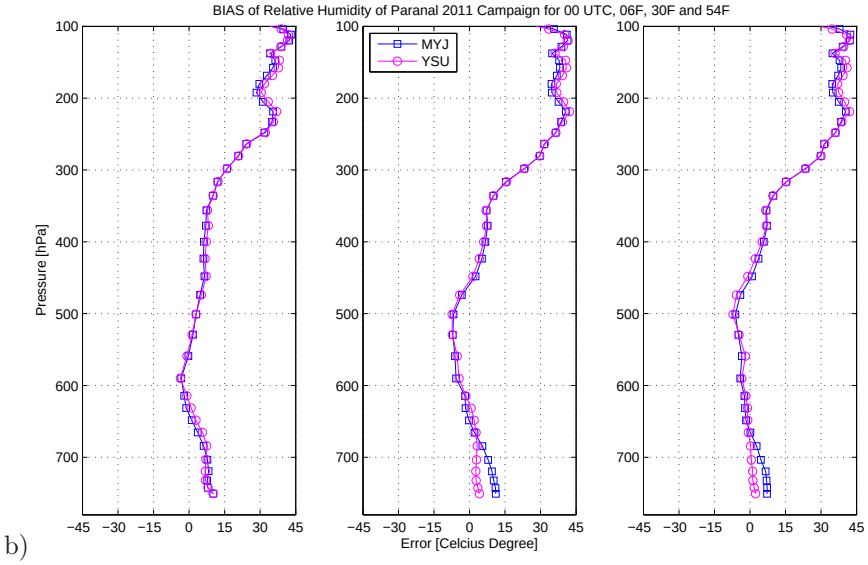

b)

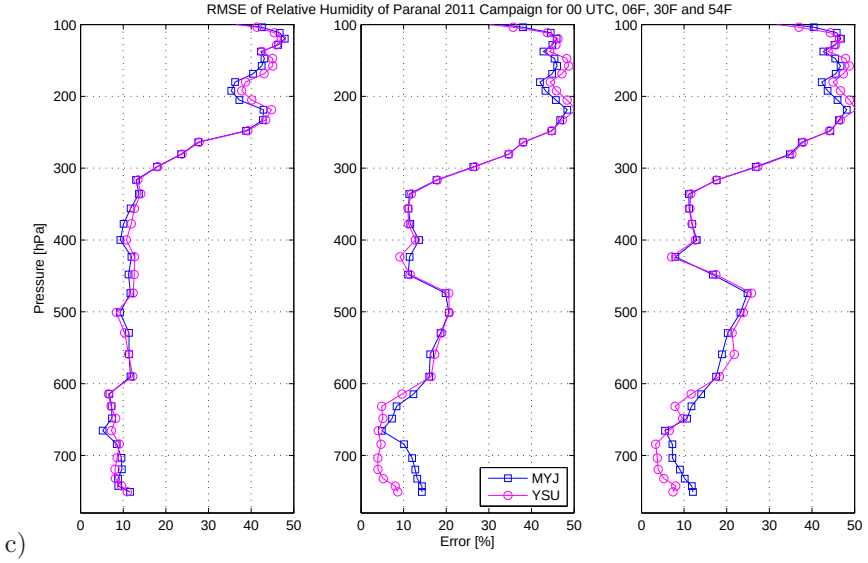

c)

Figure 22: a) Mean vertical profiles of relative humidity for radiosondes (black line), MYJ configuration (blue line) and YSU configuration (magenta line), b) vertical profile of BIAS and c) vertical profile of RMSE during the Paranal Campaign 2011.

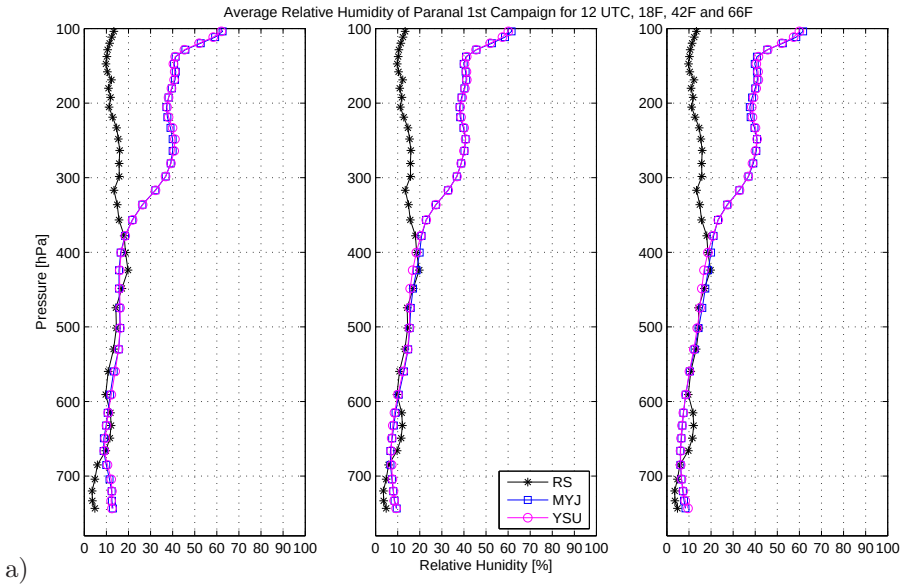

a)

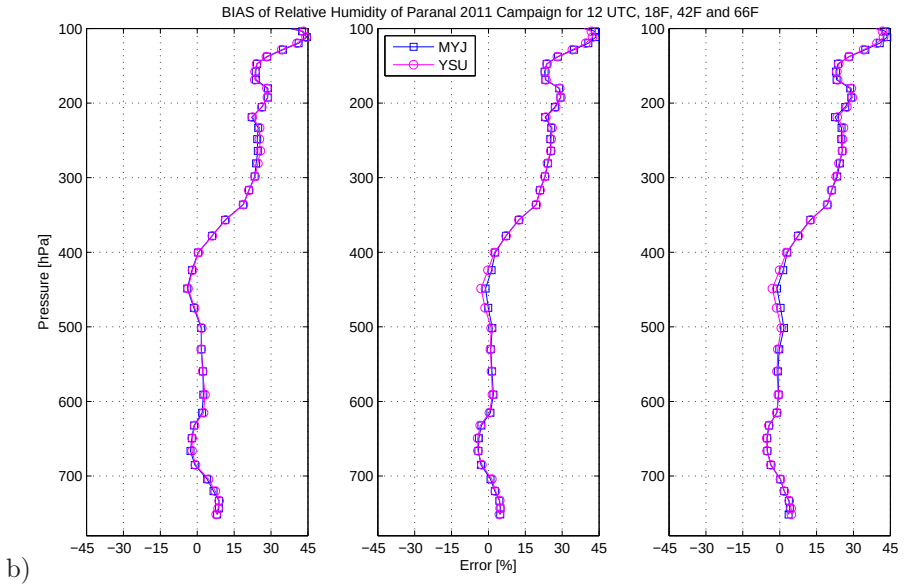

b)

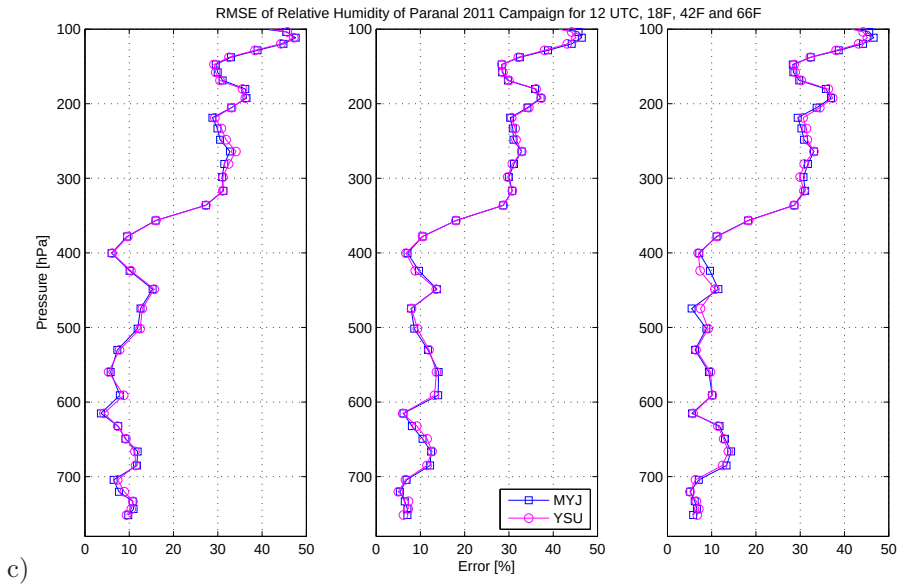

c)

Figure 23: a) Mean vertical profiles of relative humidity for radiosondes (black line), MYJ configuration (blue line) and YSU configuration (magenta line), b) vertical profile of BIAS and c) vertical profile of RMSE during the Paranal Campaign 2011.

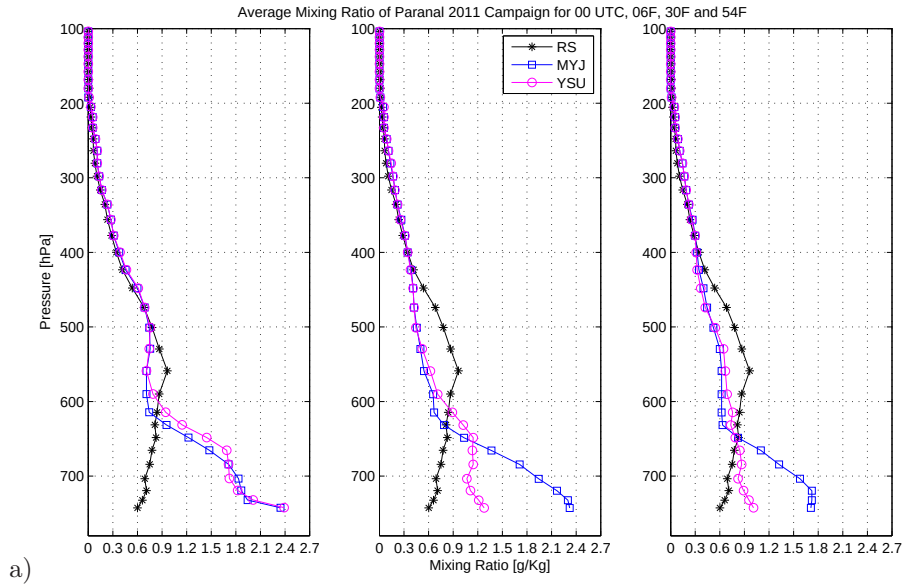

a)

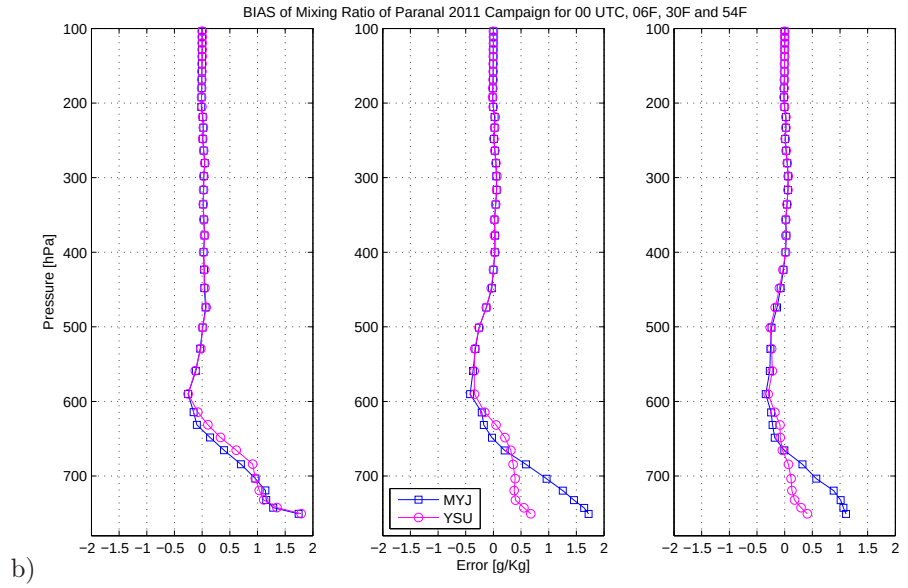

b)

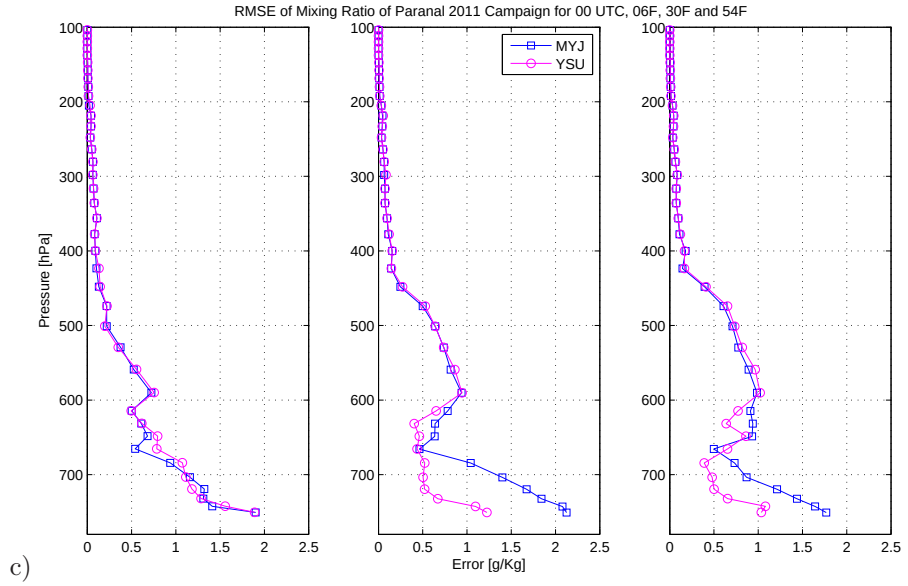

c)

Figure 24: a) Mean vertical profiles of mixing ratio for radiosondes (black line), MYJ configuration (blue line) and YSU configuration (magenta line), b) vertical profile of BIAS and c) vertical profile of RMSE during the Paranal Campaign 2011.

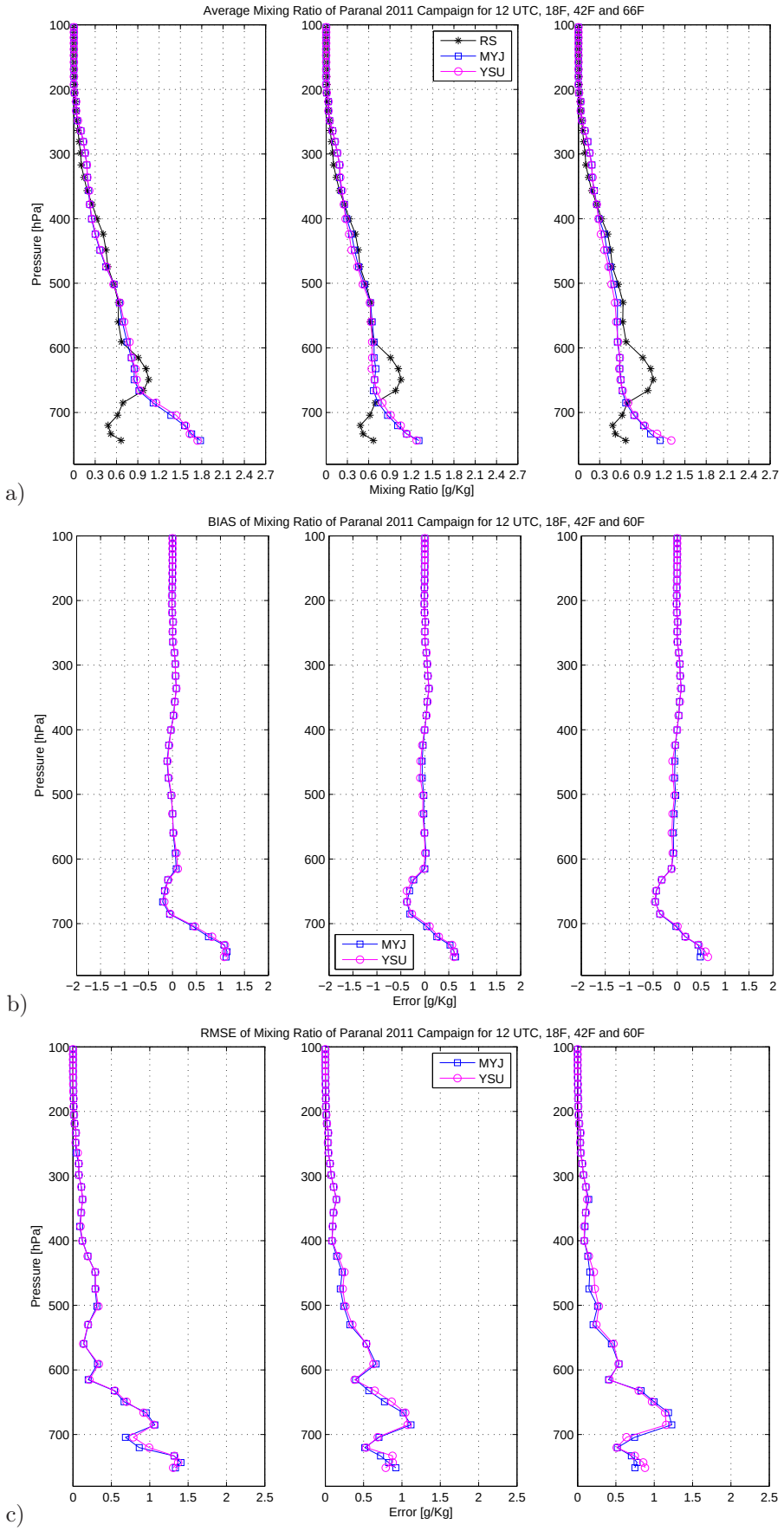

Figure 25: a) Mean vertical profiles of mixing ratio for radiosondes (black line), MYJ configuration (blue line) and YSU configuration (magenta line), b) vertical profile of BIAS and c) vertical profile of RMSE during the Paranal Campaign 2011.

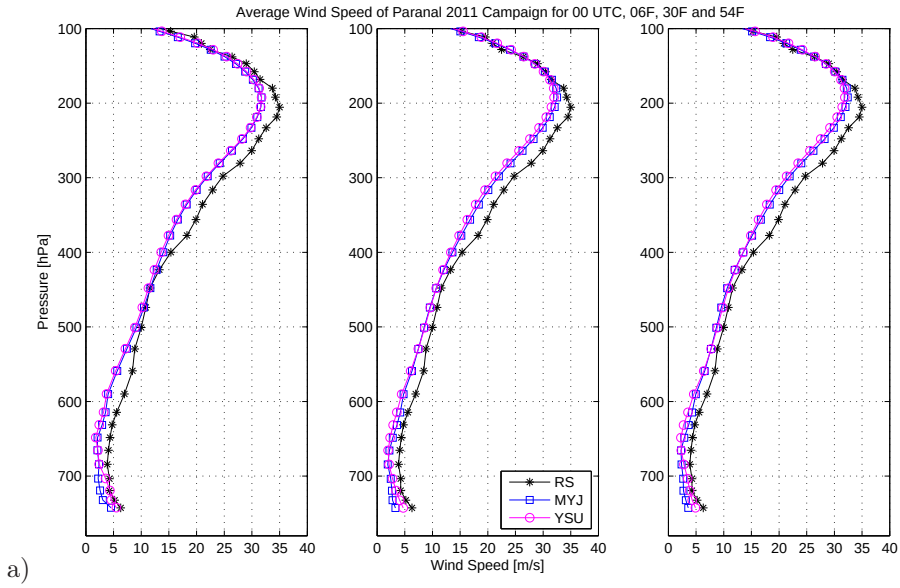

a)

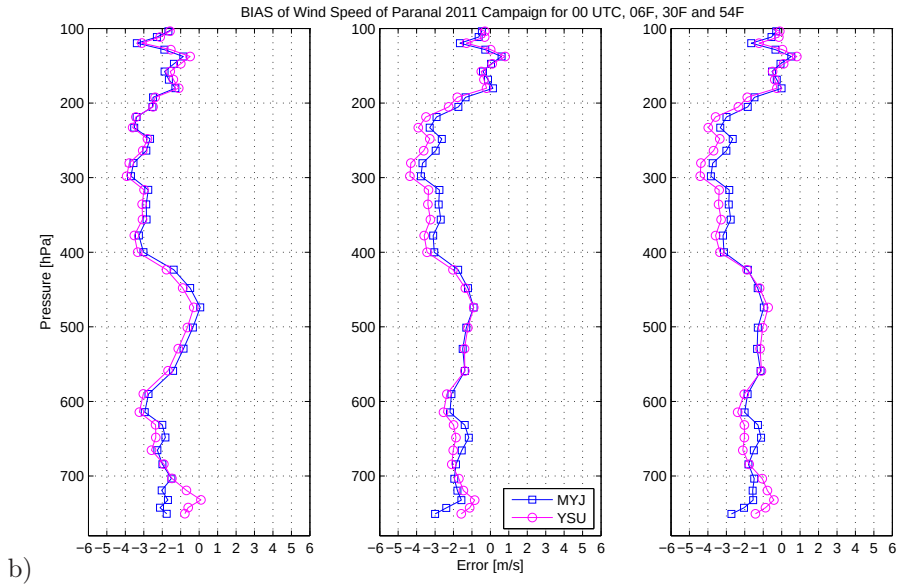

b)

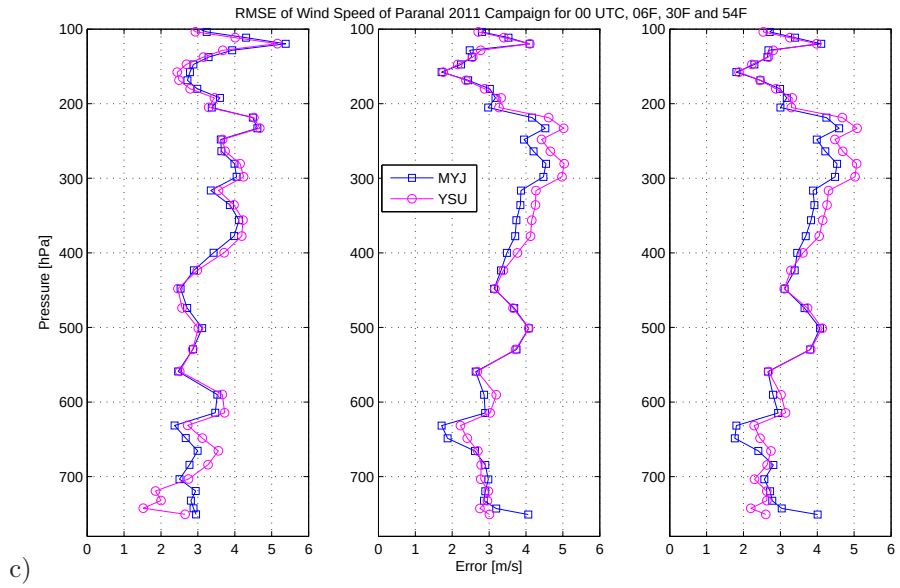

c)

Figure 26: a) Mean vertical profiles of wind speed for radiosondes (black line), MYJ configuration (blue line) and YSU configuration (magenta line), b) vertical profile of BIAS and c) vertical profile of RMSE during the Paranal Campaign 2011.

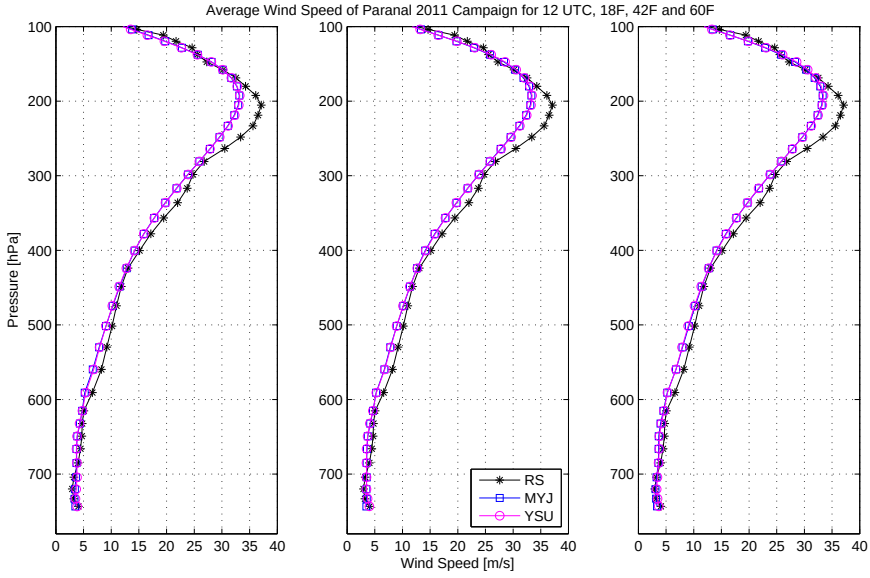

a)

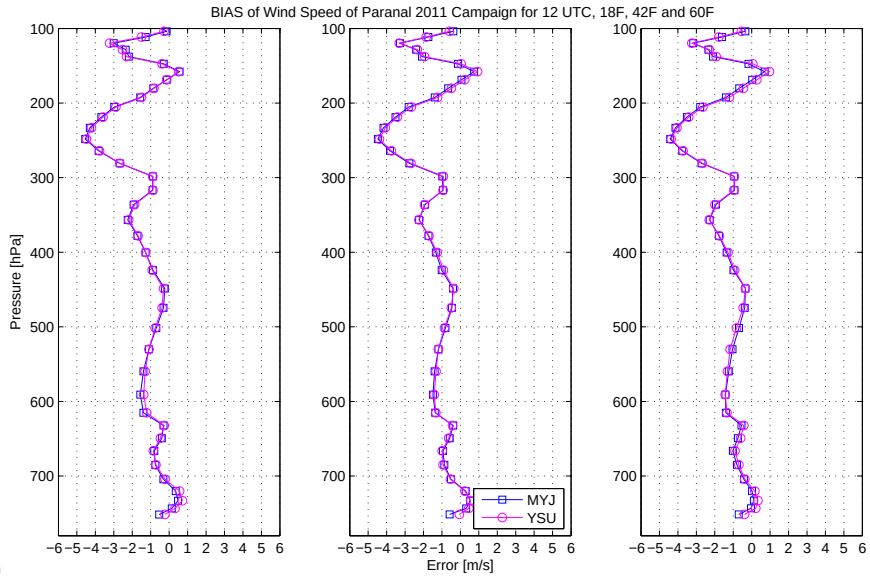

b)

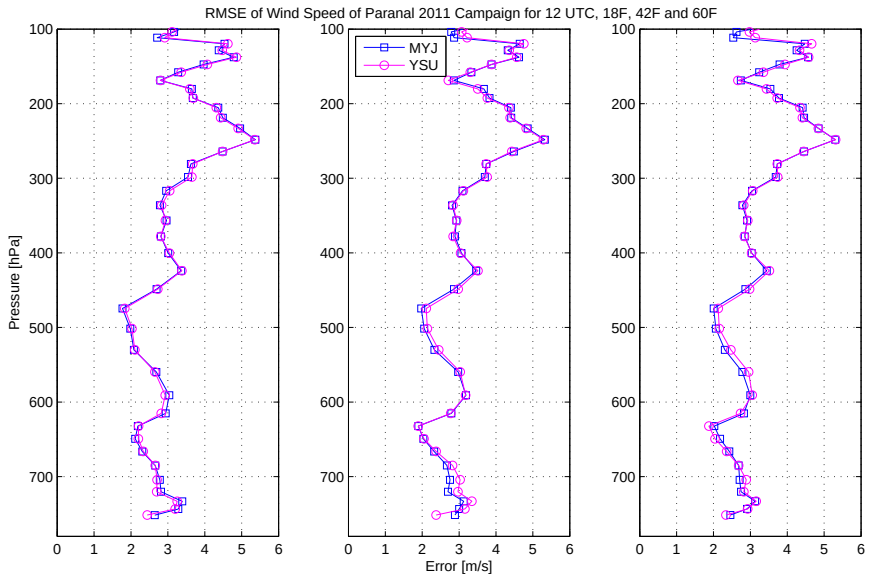

c)

Figure 27: a) Mean vertical profiles of wind speed for radiosondes (black line), MYJ configuration (blue line) and YSU configuration (magenta line), b) vertical profile of BIAS and c) vertical profile of RMSE during the Paranal Campaign 2011.

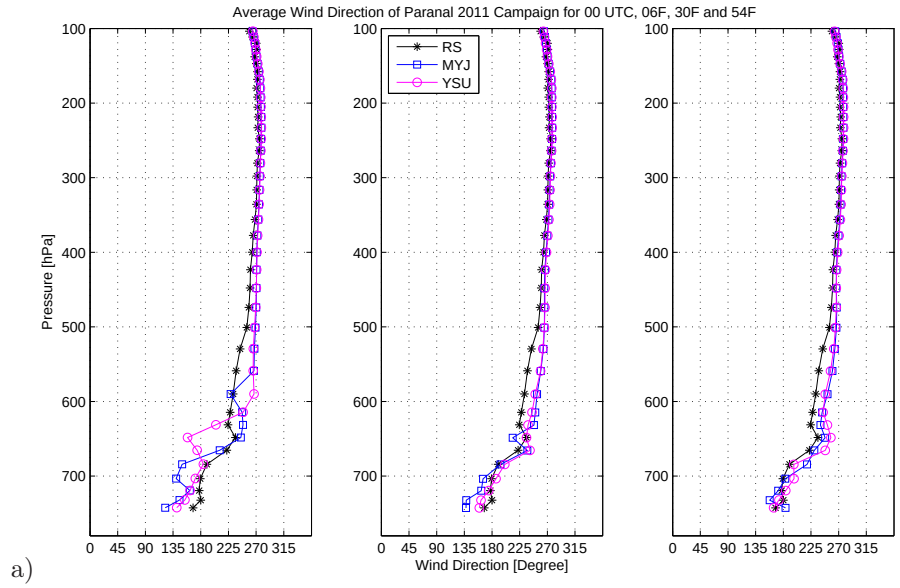

a)

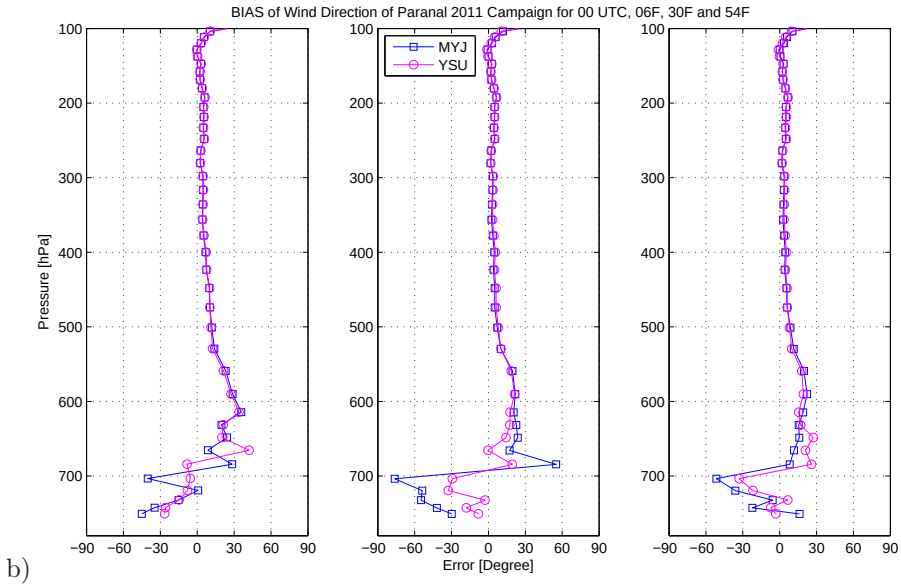

b)

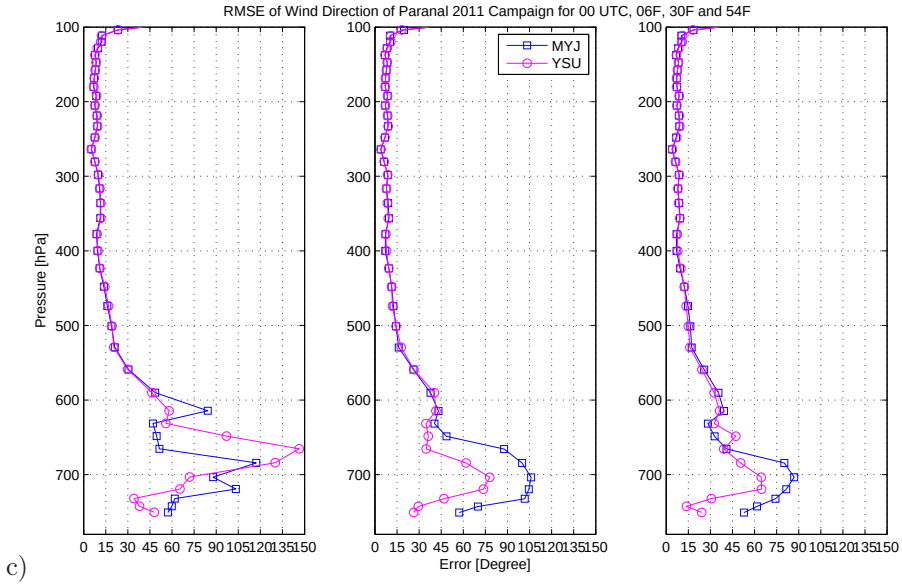

c)

Figure 28: a) Mean vertical profiles of wind direction for radiosondes (black line), MYJ configuration (blue line) and YSU configuration (magenta line), b) vertical profile of BIAS and c) vertical profile of RMSE during the Paranal Campaign 2011.

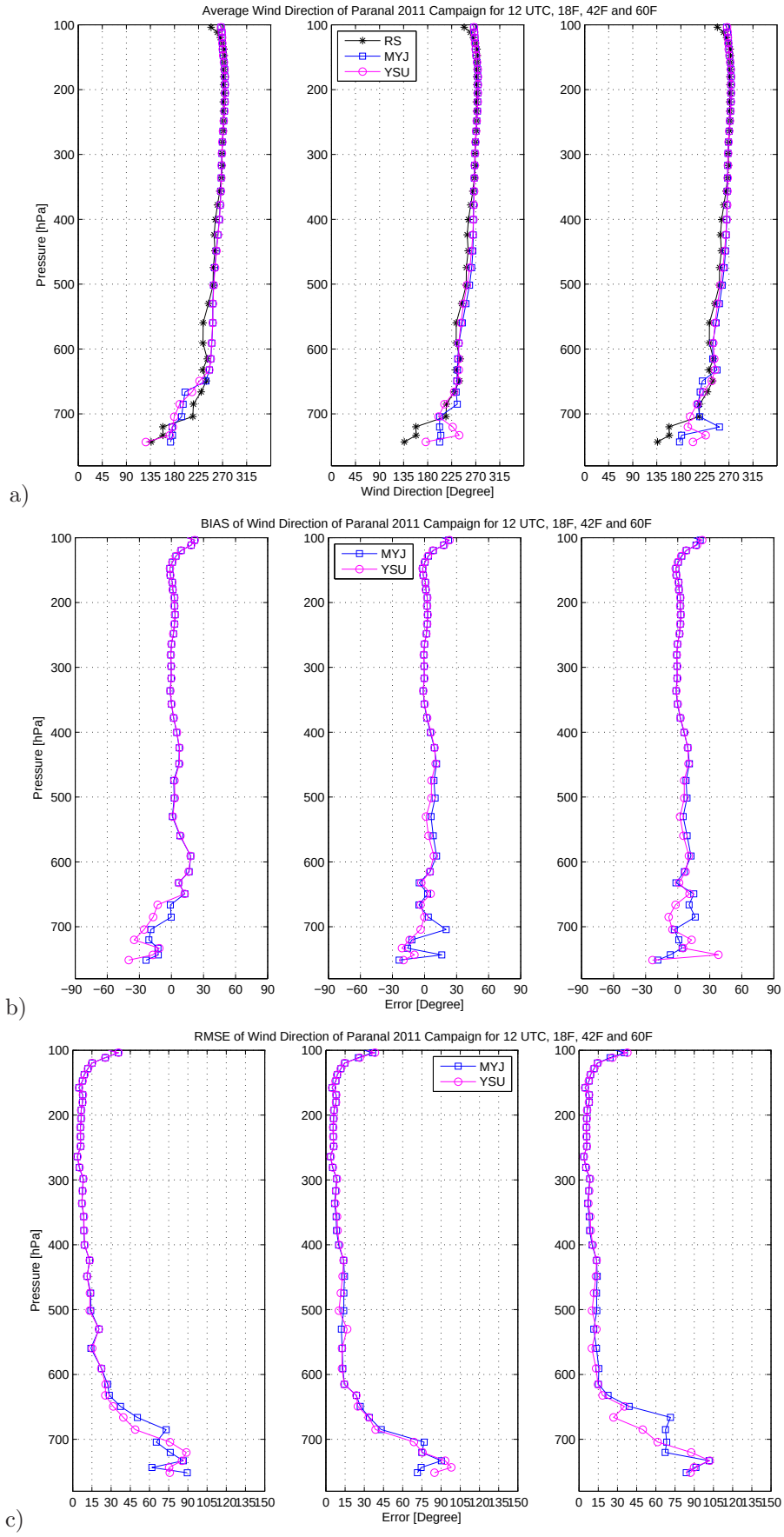

Figure 29: a) Mean vertical profiles of wind direction for radiosondes (black line), MYJ configuration (blue line) and YSU configuration (magenta line), b) vertical profile of BIAS and c) vertical profile of RMSE during the Paranal Campaign 2011.